PHYSICAL REVIEW A VOLUME 22, NUMBER 5 NOVEMBER 1980

Rayleigh scattering by neutral atoms, 100 eV to 10 MeV

Lynn Kissel*
Lawrence Livermore Laboratory, University of California, Livermore, California 94550

R. H. Pratt and S. C. Roy†
Department of Physics and Astronomy, University of Pittsburgh, Pittsburgh, Pennsylvania 15260
(Received 30 July 1979; revised manuscript received 19 June 1980)

We calculate the contribution to elastic photon scattering from an atom due to scattering off the bound atomic electrons (Rayleigh scattering). We compare predictions resulting from our numerical evaluation of the relativistic second-order S matrix in a screened central potential with other theories, particularly the form-factor approximation. We give a prescription for accurate $O(1\%)$ evaluation of total-atom Rayleigh amplitudes (summed over electrons) and present sample tabulations for lead ($Z = 82$) for energies of experimental interest in the range from 22.1 to 2750 keV. Based on our prescription we compare elastic-scattering cross sections using Rayleigh amplitudes with selected experiments and are able to remove the large factor-of-two discrepancies previously reported.

I. INTRODUCTION

Rayleigh scattering, the contribution made by bound atomic electrons to elastic photon scattering, dominates the elastic-scattering process for photon energies less than 2 MeV. Scattering is important in the energy range above the photoeffect L edge but less than 10 MeV and is among the processes (photoeffect, scattering, and pair production) primarily responsible for attenuating thin beams of photons in matter. Elastic photon scattering contributes as much as 10–20% to attenuation for high-Z atoms near but below the photoeffect K edge.[1] Interest in Rayleigh scattering has been motivated by experimental efforts to investigate other contributions to elastic scattering,[2-7] including Delbrück scattering, nuclear resonance scattering, and nuclear Thomson scattering. A number of experimenters[2-4,6,8,9] have reported large discrepancies in comparisons of measured differential elastic-scattering cross sections with those predicted by previous theories. These large discrepancies occur particularly for photon energies of 25–100 keV and 1–7 MeV.

It was John William Strutt, the third Baron Rayleigh (1842–1919) who, in his 1871 paper on the color of the sky, investigated the process with which his name is associated today.[10] Around 1906, after studying scattering of x rays by electrons, Thomson proposed the scattering cross section formula that gives the low-frequency limit for elastic photon scattering by isolated charged particles. The form-factor approximation, which was originally derived classically to correct the Thomson formula for scattering by a charge distribution rather than a point charge, is still used extensively today to predict Rayleigh-scattering amplitudes in the x-ray and gamma-ray region. Brown *et al.*[11] made important progress toward a practical method in accurately evaluating Rayleigh amplitudes by developing a numerical partial-wave solution for the second-order S-matrix element in a central potential.

This work presents a comprehensive theoretical treatment of the Rayleigh contribution to elastic photon scattering for all atoms for photon energies in the range from 100 eV to 10 MeV (Ref. 12) and develops a practical method for the accurate evaluation of total-atom Rayleigh amplitudes. The method is suitable for the production of systematic tables (Table VII). We are able to remove the large factor-of-two discrepancies between theory and experiment in this energy range. We have identified the regions where estimates of Rayleigh amplitudes based on form-factor approximation are accurate, i.e., for light atoms for photon energies well above K-shell binding and momentum transfers small compared with mc (about 20 Å^{-1}).

Section II describes the basic atomic model we use in our description of the Rayleigh-scattering process, reviews previous theoretical work which we found useful for predicting the Rayleigh amplitudes, and devotes attention to the commonly used form-factor approximation. Section III describes our numerical calculation, which is based on procedures originally developed by Brown *et al.*,[11] and subsequently applied by Johnson *et al.*[13,14] We then make extensive comparisons of these numerical predictions with existing theories. Section IV gives our prescription for the accurate $O(1\%)$ prediction of the total-atom (summed over electrons) Rayleigh amplitudes, presents sample tabulations, and discusses general features exhibited by the Rayleigh amplitudes. Section V compares theoretical elastic cross sections, using our total-atom Ray-

leigh amplitudes, with experiment and discusses the current state of agreement between theory and experiment.

II. ATOMIC MODEL AND SURVEY OF PREVIOUS THEORY

A. Atomic model

For our purposes an atom is composed of two constituents: (1) N relatively light atomic electrons distributed throughout the bulk of the atomic volume and (2) a heavy nucleus of charge Z containing the bulk of the atom's mass. (For a neutral atom $N=Z$.) Through most of the photon energy range from 100 eV to 10 MeV, the nucleus (of size 10^{-15} m) appears as a point charge; yet the energies are sufficiently high so that effects due to higher-order electron-electron correlation and consequences of other atomic features (including details of outer-electron wave functions) will be small for the photon-scattering process. In this energy range scattering is not classical, therefore the dynamics must be described with quantum mechanics. The important atomic features are described as independent atomic electrons interacting electrostatically with a single screened central potential resulting from the charge distribution of the nucleus and all the atomic electrons. The relatively high photon energies and our desire to consider heavy atoms require that we include the effects of relativity.

Elastic scattering of photons by the atom is viewed as elastic scattering by the bound atomic components (electrons and nucleus), which remain bound. Because the energy of the scattered photon is the same as that of the incident photon, we can not distinguish which of these components is responsible for the scattering. Hence, one sums the scattering amplitudes of the atomic components and then squares to obtain a scattering cross section, i.e., a coherent sum of the amplitudes. By Rayleigh scattering we mean the contribution made to elastic scattering by the atomic electrons—an atomic process.

Elastic scattering by the nucleus includes (1) nuclear Thomson scattering (scattering by the charge of the nucleus), (2) Delbrück scattering (a radiative correction to nuclear Thomson scattering and a nonclassical, nonlinear interaction of the electromagnetic fields), and (3) nuclear resonance scattering.

It is an approximation, not appropriate at very low energy, to describe the scattering by a compound system as the sum of scatterings off its constituents. Thus Gavrila,[15] studying the bound system of two particles of charge ϵ_i and mass m_i, in a nonrelativistic dipole approximation finds that the matrix element is proportional to

$$\frac{\epsilon_1^2}{m_1}+\frac{\epsilon_2^2}{m_2}-\beta^2\mu[P(\Omega_1)+P(\Omega_2)]\,,$$

where μ is the reduced mass,

$$\beta=\frac{\epsilon_1}{m_1}-\frac{\epsilon_2}{m_2}\,,\quad \frac{1}{\mu}=\frac{1}{m_1}+\frac{1}{m_2}\,,$$

and the function P vanishes at high energy and approaches $\frac{1}{2}$ at low energy. Thus at high energy, in this approximation, the cross section becomes

$$\frac{\epsilon_1^2}{m_1}+\frac{\epsilon_2^2}{m_2}\,,$$

i.e., the sum of scattering off the two free particles, while at low energy the cross section reduces to

$$\frac{(\epsilon_1+\epsilon_2)^2}{m_1+m_2}\,,$$

i.e., scattering off one (composite) particle of total mass m_1+m_2 and total charge $\epsilon_1+\epsilon_2$. For the neutral atom this vanishes. But, if we add the (high-energy) nuclear Thomson scattering to a more accurate calculation of Rayleigh scattering, we fail to get this result. This suggests that at low energy, whenever the nuclear Thomson contribution estimated in this fashion is comparable to Rayleigh scattering, the function needs to be examined more carefully.

Thus, for Rayleigh scattering from 100-eV to 10-MeV photons, we can adequately describe the atom as N noninteracting bound electrons in a relativistic self-consistent central potential. These atomic electrons are described by eigenstate solutions of the Dirac equation. The many-body electron effects are approximated by a local exchange potential of the Slater type. This description of electrons includes effects of relativity and spin, but neglects higher-order quantum electrodynamic (QED) effects such as vacuum polarization, which is partly responsible for the Lamb shift of the bound-electron energy levels.

Errors (neglected effects) in these wave functions become important for Rayleigh scattering at both ends of our energy region. Corrections due to the finite size, finite mass, and compound structure of the nucleus become more important for the description of scattering as energy increases, while the neglected many-body electron-electron correlation effects become important at lower energies.

In our approximation, the properties of the atom are determined by the atomic potential. In some situations, the Rayleigh-scattering amplitudes are sensitive to the choice of atomic potential. To obtain realistic results, we employed the self-consistent Dirac-Hartree-Fock-Slater (DHFS) poten-

tial. The DHFS potential is appropriate since it is a relatively accurate local potential, yet includes many desirable atomic features.[16] The DHFS potential includes some exchange effects, but, in the energy and atomic number ranges considered here, the results are relatively insensitive to the effects of exchange. If the Rayleigh-scattering amplitudes are very sensitive to exchange effects, then this approximate exchange model is not adequate. Exchange-dependent effects, which are not adequately described by the Slater approximation, are most pronounced for light atoms (i.e., $Z \simeq 2$) and low photon energies.

B. Form-factor approximation

The form-factor approximation for Rayleigh scattering exhibits many features of the scattering amplitude and is important for several further reasons: (1) All present tabulations of elastic-scattering cross sections[1] and attenuation coefficients[17] use this approximation to estimate the contribution made by Rayleigh scattering. (2) The approximation ties in with classical ideas, being first derived to correct the classical Thomson-scattering formula when the scattering is due to a charge distribution rather than a free point charge.[18] (3) The form factor was also derived using nonrelativistic quantum mechanics[19] followed by relativistic derivations due to Franz[20] and to Bethe.[21] (4) The form-factor approximation is particularly attractive due to its relative ease of calculation, requiring simply the evaluation of a radial integral over the atomic charge density.

The form factor $f(q)$ for a spherically symmetric charge number density $\rho(r)$ and a momentum transfer $\hbar q$ is defined as

$$f(q) \equiv \int \rho(\vec{r})\, e^{i\vec{q}\cdot\vec{r}}\, d\vec{r} = 4\pi \int_0^\infty \rho(r)\, \frac{\sin(qr)}{(qr)}\, r^2 dr\,. \tag{2.1}$$

Because we are describing the atom in a single-electron model, we may decompose the charge distribution $\rho(r)$ and also the form factor $f(q)$ into a sum of terms corresponding either to individual electrons or to a particular subshell (all electrons of fixed principal quantum number n and total angular momentum quantum number j) or a particular shell (all electrons of fixed n). Just as in electron scattering off bound electrons,[22] the form factor in elastic photon scattering corrects the point-charge scattering formula for scattering from a charge distribution. For elastic photon scattering, the relevant point-charge formula is the Thomson cross section, which describes photon scattering by a free charged particle. (For elastic electron scattering the appropriate formula is the Rutherford cross section.) The Thomson formula, being the low-energy limit of the Klein-Nishina formula for Compton scattering from free electrons, is valid classically and quantum mechanically.[23] For the case of linear photon polarizations, the two independent scattering amplitudes in the form-factor approximation for Rayleigh scattering of a photon of energy ω through an angle θ are given by

$$\begin{aligned} A_\perp^{\mathrm{FF}}(\omega, \theta) &= -f(q)\,, \\ A_\parallel^{\mathrm{FF}}(\omega, \theta) &= -f(q)\cos\theta\,. \end{aligned} \tag{2.2}$$

The magnitude of the momentum transfer q is given in mc by

$$q = 2\omega \sin(\theta/2)\,, \tag{2.3}$$

where ω is in units of mc^2 (see Ref. 24). The perpendicular $A_\perp$ and parallel $A_\parallel$ amplitudes describe the scattering of photons with polarizations perpendicular and parallel, respectively, to the plane of scattering (defined by the directions of the incident and scattered photons). In the form-factor approximation, the differential Rayleigh-scattering cross section (any other coherent processes being neglected) for unpolarized photons averaged over final polarizations may be written

$$\frac{d\sigma}{d\Omega} = \frac{r_0^2}{2}(1+\cos^2\theta)\,|f(q)|^2\,. \tag{2.4}$$

To guide us in our investigation of the form-factor approximation, we state the conditions Bethe[21] assumed in his relativistic quantum-mechanical derivation of the form-factor approximation for the Rayleigh-scattering amplitudes: (1) use of Born approximation for intermediate states (electron propagator) thus ignoring binding effects (this is a low-Z high-energy assumption, requiring energy large compared with binding), and (2) momentum transfers small compared to mc.

The range of validity of the form-factor approximation for the description of elastic photon scattering by bound electrons is limited. For scattering by low-energy photons, effects of binding are crucial; they are neglected[25] by the form-factor-corrected Thomson formula, because the Thomson formula describes scattering from free electrons. At higher energies one might expect that binding effects would become less important and that scattering would approach that for free electrons. In fact, $O(Z\alpha^2)$ corrections remain at all energies and angles. For a given atomic electron, the form-factor approximation is not valid for larger angles (high momentum transfers) or lower energies (compared with electron binding). With decreasing energy the approximation first fails for inner electrons (of larger binding energy), which, however, give a dominant contribution at larger

momentum transfers (larger angles at higher energies). In addition, corrections due to relativity have been neglected, again implying deviations of the form factor for the inner shells of heavy atoms or for high photon energies.

C. Qualitative features predicted by the form-factor approximation

Although form-factor predictions are often wrong in quantitative detail, their qualitative features give considerable insight into the behavior of the Rayleigh amplitudes.

We may better understand the behavior of the total-atom form factors, $f(q)=\sum f^i(q)$, by considering the behavior of its components $f^i(q)$, contributed by each particular electron, subshell, or shell, as a function of the momentum transfer. For zero momentum transfer, the integral for a subshell form factor reduces to an integral over the corresponding subshell charge density and is equal to the number of electrons in that subshell. As the momentum transfer increases, the value of $f^i(q)$ remains approximately constant until momentum transfers corresponding to the typical momentum (q_{typ}) of electrons in that subshell is reached. We may estimate this momentum, at least for inner subshells, using the Bohr radius of an electron of principal quantum number n

$$q_{\text{typ}} \simeq \frac{1}{a_n} = \frac{Z\alpha mc}{n^2\hbar} . \tag{2.5}$$

For momentum transfers larger than this inverse Bohr radius, the magnitude of the form factor becomes small. For nodeless subshells (such as the K shell), the value of the form factor for $q>q_{\text{typ}}$ decreases monotonically. For subshells with nodes (such as the L_{I} subshell), there is a region of more rapid variation or oscillation for $q>q_{\text{typ}}$ before reaching the asymptotic region where $f^i(q)$ decreases monotonically. We may easily determine the large-q behavior of the form factor for a given atomic electron subshell. Nonrelativistically, the radial-charge number density of a given bound-electron subshell is given by

$$\rho(r)=[N_e r^l s(r)]^2 , \tag{2.6}$$

where N_e is the bound-state normalization and l is the orbital angular-momentum quantum number. For small radial distances, we may write[26]

$$s(r)=1-\frac{Z\alpha r}{l+1}+\cdots , \tag{2.7}$$

so that for large q, the single-electron form factor becomes

$$\lim_{q\to\infty} f^i(q)=(-1)^l \frac{8\pi Z\alpha N_e^2(2l+2)!}{(l+1)q^{2l+4}} . \tag{2.8}$$

The subshell form factor is found by multiplying Eq. (2.8) by the number of electrons in the subshell. For large q, $f^i(q)$ decreases rapidly with q (but most slowly for $l=0$), and is larger for heavy atoms where Z and N_e are larger.

We now predict the relative importance of a given subshell in the total-atom form factor. For small momentum transfers, each subshell contributes to the total-atom form factor proportional to the number of electrons in that subshell. As the momentum transfer increases, the contribution of each subshell remains approximately constant (equal to the number of electrons in that subshell) until the typical momentum of electrons in that shell (estimated by the inverse of the average size of that subshell) is reached. Beyond that typical momentum, the contribution to the total-atom form factor from that particular subshell decreases rapidly. As the momentum transfer increases, the contributions to the total-atom form factor of more and more of the outer electrons become small as the momentum transfer increases beyond their typical momenta. This process continues until the K shell's typical momentum ($Z\alpha$) is exceeded. Beyond this point contributions to the total-atom form factor due to all subshells are monotonically decreasing. In this asymptotic region the s states ($l=0$) dominate, with the inner shells yielding the largest contribution (due to the larger N_e). Thus, for a heavy element such as lead, the form-factor approximation predicts that the K shell dominates at large momentum transfers, with the next largest contribution coming from the L_{I} subshell (contributing about 15% as much as the K shell for lead). We display partial-atom form factors and total-atom form factors as a function of momentum transfer in Fig. 1 for lead ($Z=82$) and aluminum ($Z=13$). Note that for small q, the contribution to $f(q)$ from a given shell is independent of Z, while the onset of the drop-off (q_{typ}) for each shell is Z dependent.

The differential scattering amplitudes Eq. (2.2) are simply obtained from the form factor. The range of momentum transfers possible for a fixed photon energy ω are $0\leq q\leq 2\omega$. Thus for low photon energies, the form factor predicts little variation in the differential scattering amplitudes beyond the explicit $\cos\theta$ dependence. For high photon energies, the form factor is equal to the number of electrons in the forward direction but becomes very small at the backward angles, giving a highly forward-peaked angular distribution. However, since $f(q)$ only dips by a factor of four between 90° and 180° [it drops as q^{-4} with $q=2\omega\sin(\theta/2)$], while $1+\cos^2\theta$ increases by a factor of two, even in the high-energy limit the cross section equation (2.4) will not dip by more than a factor of eight across

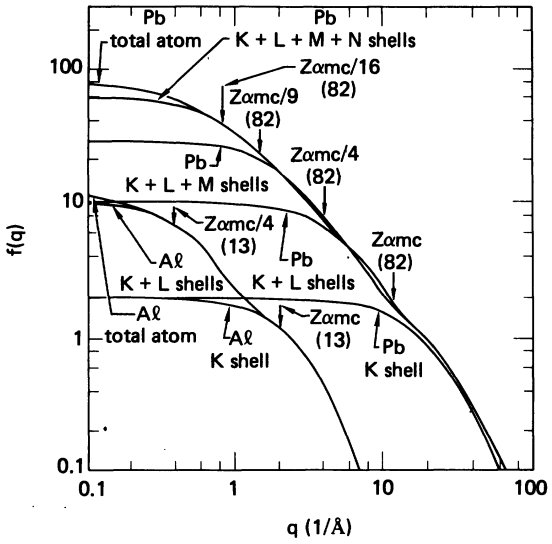

FIG. 1. Values of the form factor for aluminum (Z =13) and lead (Z=82) as a function of momentum transfer in inverse Å. The form factors used to produce these curves are derived from DHFS wave functions.

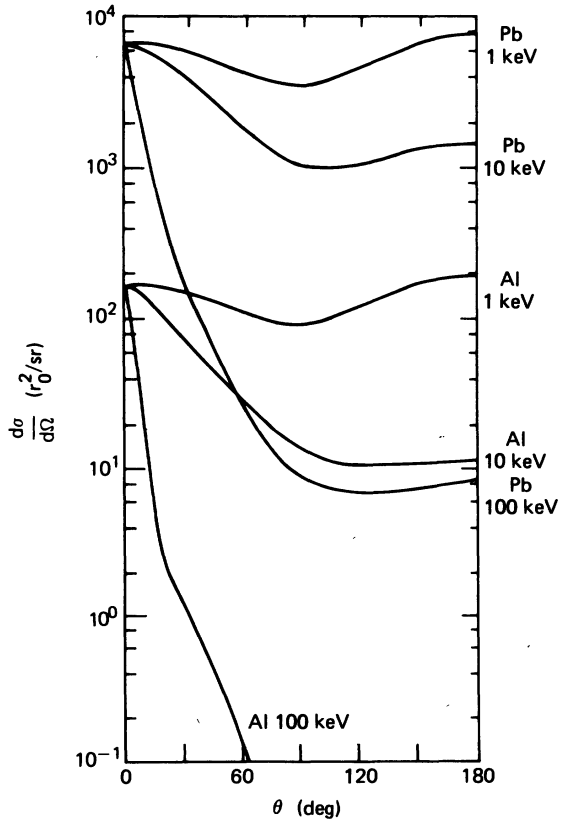

FIG. 2. The sum of squared scattering amplitudes in the form-factor approximation, Eq. (2.4), as a function of scattering angle. Note the more isotropic lower-energy scattering and the extremely forward-peaked higher energy scattering.

the backward hemisphere. For small q, the cross section will go as Z^2, while for large q (remembering that N_e^2 for the K shell goes as Z^3) it will go as Z^8. Figure 2 displays the total-atom differential cross sections derived from the form factors of Hubbell *et al.*[27] for 1-, 10-, and 100-keV photons for aluminum and lead. We see the behavior of the form factor as a function of the momentum transfer translated into the differential scattering cross section as a function of scattering angle θ.

The form-factor approximation also predicts the importance of electron screening of the nuclear charge (i.e., sensitivity to the choice of atomic potential). For small momentum transfers the form factor reduces to the number of electrons, which is independent of the potential used and suggests that screening effects are small. For large momentum transfers, small radial distances are most important. For small radial distances, screening corrections to the Coulomb wave functions appear only in their normalizations.[26] Thus the form-factor approximation predicts that, for large q, screening effects in the matrix elements can be expressed as the squared ratio of screened to unscreened bound-state wave-function normalizations.

D. Some modifications and corrections to form-factor approximation

A correction to the form-factor approximation was suggested by Franz[20] in his original relativistic derivation of the form-factor description of scattering. Brown and Mayers[11] compared this modified form factor due to Franz with their numerical scattering amplitudes and found that it gave improved results.[28] This modified form factor is given for an atomic electron with radial number density $\rho(r)$ as

$$g^{\dagger}(q) = 4\pi \int_0^{\infty} \rho(r) \frac{\sin(qr)}{qr} \left(\frac{1}{1 - \epsilon - V(r)} \right) r^2 dr , \tag{2.9}$$

where ϵ is the electron binding in mc^2 energy and $V(r)$ is the electrostatic potential. The total-atom modified form factor is found by summing $g^{\dagger}(q)$ over all electrons. The additional denominator factor has its origin in the Green's-function propagator of the intermediate states and represents a binding correction. It will be shown that this modified form factor tends to remove the $(Z\alpha)^2$ errors found at high energies in the ordinary form-factor approximation.

Levinger[21] considered small-angle scattering of gamma rays by bound electrons. He derived the corrections to the form-factor approximation in the near-relativistic region by expanding the scat-

tering matrix element in powers of (q/mc) while assuming that the photon energy was large as compared with electron binding. He found that relativistic effects tended to increase the value from the form-factor predictions by an amount of the order of $(Z\alpha q/mc)f(q)$, which is small for small Z. This prediction—as does that of the form-factor approximation—neglects the effects of binding for the electron.

Brown and Woodward[29] investigated the importance of binding of the electron for high-energy scattering by expanding the QED electron propagator in a Born series. The zeroth-order term of this series yields the usual form-factor approximation under the additional assumption that $q/mc \ll 1$. (The previously mentioned work of Levinger[21] considers the remaining parts of this zeroth-order term for $q/mc \leq 1$.) Brown and Woodward studied the higher-order terms of this Born expansion and found that these terms dominated the scattering for $q/mc \gg 1$.

All derivations of the form-factor approximation have assumed that $\omega \gg \epsilon$ and so treat the electron as a free particle. But in many cases of interest the photon energy is comparable to the electron binding energy, especially for medium- and high-Z atoms where K-shell binding is tens of kilovolts. The simple form of the Rayleigh-scattering amplitudes in the form-factor approximation, given by Eq. (2.2), may be retained by replacing the form factor $f(q)$ by a scattering factor F given by

$$F = f(q) + (\Delta f') + i(\Delta f''). \tag{2.10}$$

The corrections $\Delta f'$ and $\Delta f''$ have been referred to as the dispersion corrections to the form factor, anomalous-scattering factors, or anomalous-dispersion corrections. The word "anomalous" alludes to the observed rapid variations of the photon energy around $\omega = \epsilon$. Chapter IV of James[18] discusses previous work on this subject. Cromer and Liberman[30] performed numerical calculations of the anomalous-scattering factors using DHFS wave functions. However, these anomalous-scattering factors have been derived for the case of forward scattering only (i.e., $\theta = 0$). It has been the practice to transform these zero-angle corrections to nonzero values of θ by multiplying the zero-angle value of $\Delta f'$ and $\Delta f''$ for each electron by its corresponding form factor, which is unity at $\theta = q = 0$. This procedure of transforming the zero-angle corrections to other angles has not been justified.

E. The high-energy limit

Special attention has been devoted to the scattering of very-high-energy photons by bound electrons. In the forward direction, the form-factor approximation reduces to scattering off a free charge. At low energies, binding effects will clearly introduce large modifications, but in the high-energy limit it was historically expected that scattering by the bound electrons would approach the free-particle value in the forward direction. Goldberger and Low[31] considered high-energy-limit corrections to the scattering in the forward direction and demonstrated that corrections at high energy remain finite and increase with atomic number, on the order of $(Z\alpha)^2$. These corrections reduce the scattering amplitudes in comparison with the form-factor prediction, especially for heavy atoms. Florescu and Gavrila[32] extended these results to finite momentum transfers for the Coulomb potential in the high-photon-energy limit. From their work they could rederive the form-factor approximation in the small-$Z\alpha$ limit under the usual $q/mc \ll 1$ assumption.

F. Nonrelativistic Coulomb dipole approximation

Further features of the Rayleigh amplitude at low energy, not exhibited in the form-factor approximation, are displayed in the nonrelativistic dipole approximation. Exact analytic expressions were obtained by Gavrila[33] for the nonrelativistic dipole approximation in the Coulomb potential for the K shell, and for L-shell electrons by Costescu.[34] Only the K-shell results have been tabulated. This work, which neglects screening, is nonetheless interesting when the incident photon energy is less than, or of the order of, the electron's binding energy. Since electron binding is included, it yields useful insights in a region where the form factor is completely inadequate.

For photon energies below the photoeffect K edge, the Coulomb K-shell dipole amplitudes of Gavrila exhibit singularities at energies corresponding to differences of bound-state energies between the K shell and the higher shells. The analogous L-shell amplitudes exhibit similar singularities, including one corresponding to a transition downward to the K shell. While the singularities are unphysical (due to neglecting the finite width of atomic levels), resonance is expected at those energies that correspond to bound-bound transitions from an occupied to an unoccupied bound state. In the single-electron model, transitions will be calculated even to filled levels. However, resonant contributions connecting two occupied orbitals (as $K \rightarrow L \rightarrow K$ and $L \rightarrow K \rightarrow L$ in this example) cancel identically when the scattering amplitudes are summed over all populated levels, provided that a single potential is used for all calculations. The resulting amplitudes are equivalent to those obtained by considering transitions only to unoc-

cupied states. Resonance is expected only when the photon energy approaches the difference between an occupied and unoccupied orbital. However, the existence of unphysical resonances in the single-particle amplitudes and their cancellation when the amplitudes are summed over all electrons in the atom demonstrates that we must be careful in our choice of single-electron amplitudes for multielectron atoms, especially at low energy. Use of formalisms for inner electrons that explicitly include electron binding (and thus include these resonant effects) together with formalisms such as the form-factor approximation (which neglects some effects of binding) to estimate contributions of the outer electrons will fail in some cases. We discuss this further in Sec. IV.

G. Numerical calculations

Since the mid-1950's, attempts have been made to provide a more accurate evaluation of the Rayleigh-scattering amplitudes. These numerical methods start with the second-order S matrix (the lowest order in the relativistic theory for which the process is nonvanishing), expand the Green's function as a sum over all states of the atomic potential $V(r)$, and expand the photon wave functions in a multipole series (Fig. 3). The radial Green's function is not directly computed, but the solution of an inhomogeneous wave equation is found that is equivalent to the integral over the Green's function, one of the photon vertices, and one of the bound states. Brown *et al.*[11] considered the K shell of mercury ($Z=80$) using the Coulomb potential and calculated the scattering amplitudes for incident photons of energies 164, 327, 654, and 1308 keV. (The 164-keV calculation initially used a screened potential, but was later recalculated using the Coulomb potential; it was found that screening corrections were unimportant.) The 1308-keV calculation showed poor agreement with experiment, but, since the Rayleigh amplitudes are not the only important elastic amplitudes at this energy, the source of the discrepancy was not clear. Cornille and Chapdelaine[35] used Brown's procedure to calculate the scattering amplitudes for the K shell of mercury for a photon energy of 2620 keV.

Johnson and Feiock[13] extended Brown's procedure, obtaining results with the more realistic DHFS wave functions. Performing calculations for the noble gases He, Ne, Ar, Kr, Xe at 1–10 eV, where the cross sections are dominated by contributions from the outer-shell electrons, they were able to evaluate the electric and magnetic susceptibilities of the atom as well as the dispersion of these susceptibilities as the frequency increased. They interpreted disagreements with

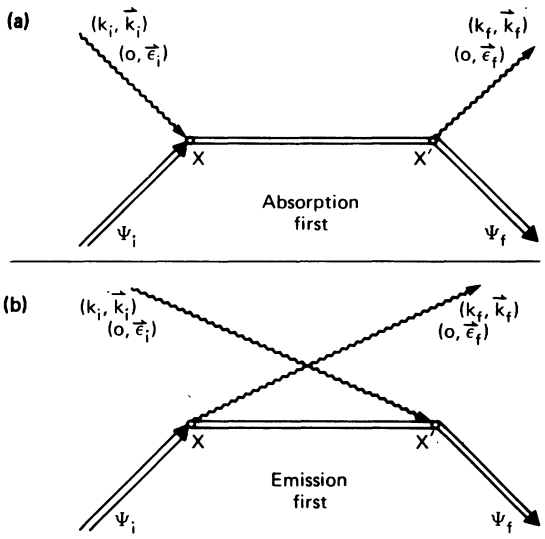

FIG. 3. Furry diagrams that depict the two scattering processes contributing to the second-order S matrix for photon scattering by electrons. The absorption first process (a) corresponds to an initial-state electron ψ_i absorbing the initial-state photon of energy k_i. At some later time the electron leaves the intermediate state and enters the final state ψ_f by emitting the final-state photon of energy k_f. In the emission-first process (b), the order of initial-state photon absorption and final-state photon emission are reversed. For Rayleigh scattering $\psi_i=\psi_f$ and $k_i=k_f$. However, it is not usually true that $\vec{k}_i=\vec{k}_f$.

experiment as due to the neglect of correlations.

Lin *et al.*[13] included higher-order electron-electron correlation contributions coming from the fourth-order S matrix. For helium ($Z=2$) they found that the use of DHFS wave functions in their lowest-order calculation introduced contributions to the fourth-order S matrix that tended to cancel other fourth-order contributions; i.e., the inclusion of the approximate exchange potential of the DHFS potential approximately represents the electron-electron interaction. The importance of the residual fourth-order correlation effects, which are expected to be largest for the case of helium, decreased as the incident photon energy increased. For total cross sections, these effects of correlations had become less than 10% by 100 eV, less than 5% by 200 eV, and less than 1% by 400 eV. Correlation corrections to the angular distributions were insignificant by about 1 keV. Correlation effects are expected to be more correctly included within the DHFS model for the inner shells of heavier atoms due to the larger number of electrons present, better justifying the statistical assumptions of the Slater exchange model. In addition, the importance of correlations is expected

to decrease as the atomic number increases. Therefore, correlation effects, neglected by considering only contributions of the second-order S matrix with DHFS potentials, are expected to be small in most cases for the heavier atoms and higher photon energies.

Johnson and Cheng[14] used this extension of the numerical procedure of Brown for the second-order S matrix in a more systematic study for relatively heavy atoms ($30 \leq Z \leq 82$) for photon energies 100 through 900 keV. They included contributions of some higher shells and were able to obtain satisfactory agreement (5–20%) between theory and experiment in this energy range. They attributed the remaining 5–20% discrepancies to contributions made by outer electrons which they neglected. Due to limitations of the computer codes used in their work, they did not calculate the scattering amplitudes for other energies or lighter atoms. The present work builds upon, and has benefited from, this sequence of previous numerical calculations.

III. OUR CALCULATIONS AND THE VALIDITY OF SIMPLER THEORETICAL APPROACHES

We have written a new code for the numerical evaluation of the second-order S matrix for the Rayleigh-scattering amplitudes based on the extension of the formalism of Brown *et al.*[11] and by Johnson *et al.*[13] Our review of previous theories in Sec. II shows that this is the most rigorous formalism now available for the practical evaluation of Rayleigh-scattering amplitudes for multielectron atoms over an extended energy range, even though it is difficult to program and costly in computer time for heavy atoms with many electrons. Our objective is to work toward a prescription for the accurate $O(1\%)$ prediction of total-atom Rayleigh-scattering amplitudes which relies as much as possible on the simpler theories. (Section IV describes this prescription and presents sample tabulations of the Rayleigh amplitudes.)

This section is in four parts. Section III A briefly discusses our numerical calculation of the inner-shell Rayleigh amplitudes. We also mention some of the numerical checks applied in verifying the accuracy of our codes. Section III B compares our predictions with other theoretical work. Section III B further tests our predictions and gives us greater confidence in the results. (These results are not merely a duplication of previous work since they include discrepancies that we are able to explain.) Section III C is a careful investigation of the validity of the form-factor approximation, modified form-factor approximation, anomalous-dispersion corrections to the form factor, and high-energy-limit formulas. In particular, we attempt to determine in which regions of parameter space (Z, ω, θ, etc.) these important simpler theories are valid. Lastly, Sec. III D notes some of the general features observed in the Rayleigh-scattering amplitudes (i.e., effects of screening and relativity, the relative contribution of various atomic shells and the dependence on photon multipole).

A. Our numerical calculation of inner-shell contributions to the Rayleigh amplitude

The matrix element we evaluate for Rayleigh scattering of a photon of energy ω by a bound electron in the state $n\kappa m_j$ of energy $E_{n\kappa} = 1 - \epsilon_{n\kappa}$ is

$$M_{n\kappa m_j} = \int_p \left(\frac{\langle n\kappa m_j | A^* | p \rangle \langle p | A | n\kappa m_j \rangle}{E_{n\kappa} - E_p + \omega} + \frac{\langle n\kappa m_j | A | p \rangle \langle p | A^* | n\kappa m_j \rangle}{E_{n\kappa} - E_p - \omega} \right), \quad (3.1)$$

where $\int_p$ is the generalized sum-integral over all states p of energy E_p.[36] The operators A (A^*) represent absorption (emission) of a photon of energy ω. We expand these photon operators A, A^* in multipoles and all electron wave functions in partial waves. Following Johnson *et al.*[13] we define positive and negative energy perturbations of the bound state

$$|n\kappa m_j +\rangle = \int_p \frac{|p\rangle \langle p | A | n\kappa m_j \rangle}{E_{n\kappa} - E_p + \omega},$$
$$\langle n\kappa m_j - | = \int_p \frac{\langle n\kappa m_j | A | p \rangle \langle p |}{E_{n\kappa} - E_p - \omega}. \quad (3.2)$$

These perturbed orbitals satisfy an inhomogeneous Dirac equation. The inhomogeneous terms are proportional to the products of the bound-state radial wave function and spherical Bessel functions (from the photon operators). The Rayleigh-scattering amplitudes for scattering of linearly polarized photons from a given filled atomic subshell may be written as (in units of classical electron radii)

$$A_{\parallel}^R(\omega, \theta) = -\sum_{J=1}^{\infty} \left(\frac{2J+1}{2} \right) \left[\left(P_J^0(x) - \frac{P_J^2(x)}{J(J+1)} \right) X_J^1(\omega) + \left(\tfrac{1}{2}[P_{J-1}^0(x) + P_{J+1}^0(x)] + \frac{P_{J-1}^2(x) + P_{J+1}^2(x)}{2J(J+1)} \right) X_J^0(\omega) \right],$$
$$A_{\perp}^R(\omega, \theta) = -\sum_{J=1}^{\infty} \left(\frac{2J+1}{2} \right) \left[\left(P_J^0(x) - \frac{P_J^2(x)}{J(J+1)} \right) X_J^0(\omega) + \left(\tfrac{1}{2}[P_{J-1}^0(x) + P_{J+1}^0(x)] + \frac{P_{J-1}^2(x) + P_{J+1}^2(x)}{2J(J+1)} \right) X_J^1(\omega) \right]. \quad (3.3)$$

The associated Legendre polynomials $P_A^B \cos\theta$ contain all the angular dependence of the scattering amplitudes. The functionals $X_J^\lambda(\omega)$ contain all the dependence on energy and are found numerically by performing radial integrals over the solutions of the perturbed orbitals Eq. (3.2).[37] The eigenvalues J, λ correspond to the photon's multipolarity and parity, respectively.

We analytically summed the scattering amplitudes over all electrons in a filled atomic subshell to suppress the more complicated dependence of the amplitudes on the magnetic quantum number m_j. If it proves important, we can recover the m_j dependence of the scattering amplitudes at a later date. However, in what follows we will always ignore this dependence and discuss scattering by filled atomic subshells only.

We followed closely the formalism of Johnson *et al.*,[13] but in our codes we implemented two important improvements that remove limitations in the range for which their codes were valid. First, we explicitly programmed the negative-energy continuum solution for the perturbed orbital $\langle n\kappa m_j -|$ of (3.2), which occurs for energies ω greater than $2mc^2 - \epsilon$. (At lower energies this orbital satisfies bound-state boundary conditions.) Second, we employed a variable-step-size technique which allows us to cover a wider range of photon energies and atomic numbers with one code. Truncation-error estimates automatically adjust step sizes during quadrature and integrations of differential equations.

We made explicit calculations for energies above about 1 keV through about 3 MeV, for various atomic numbers $Z \leq 92$, and K, L, M, N shells, but expect that our code is valid for still higher and lower energies. The code accepts as input several choices of numerical or analytic central-field atomic potentials. We used the self-consistent Dirac-Hartree-Fock-Slater potentials most extensively (with the Kohn-Sham exchange model[38]), but also obtained predictions for the Coulomb potential. The intermediate case of Rayleigh scattering off ions was not investigated, but has been explicitly allowed for in our code.

We performed many checks on our codes to ensure their accuracy. Special functions, such as the spherical Bessel functions, Legendre polynomials, and Clebsch-Gordan coefficients, were checked against existing tabulations.[39,40] Large- and small-distance properties of our solutions of the radial Dirac equation were compared with known analytic properties (such as phase shifts, normalizations, amplitudes, etc.) in the case of the Coulomb potential.

Another partial check of our results for each subshell by the optical theorem relates the imaginary part of the forward-scattering amplitude to the total cross section. Since we are considering contributions from the second-order S matrix, we observe the following relation between the imaginary part of our Rayleigh forward amplitude and the first-order one-photon absorptive processes of photoeffect and pair production. For photon energy $\omega < \epsilon$ the imaginary part of the forward amplitude is zero. For photon energies greater than the binding energy of the subshell ϵ but less than $2mc^2 - \epsilon$, the imaginary part of the forward-scattering amplitude equation (3.3) is related to the total photoeffect cross section $\sigma_{pe}(\omega)$ (measured in units of electron Compton wavelength squared $\lambda\!\!\!^{-2}$) by

$$\mathrm{Im}A_\perp^R(\omega, \theta = 0) = \mathrm{Im}A_\parallel^R(\omega, \theta = 0) = \frac{\omega}{4\pi\alpha}\sigma_{pe}(\omega) . \quad (3.4)$$

For photon energies greater than $2mc^2 - \epsilon$, the imaginary part of the forward-scattering amplitude is related to the total photoeffect cross section and the total one-photon bound-electron pair-creation cross section $\sigma_{pc}(\omega)$ (measured in $\lambda\!\!\!^{-2}$) by

$$\mathrm{Im}A_\perp^R(\omega, \theta = 0) = \mathrm{Im}A_\parallel^R(\omega, \theta = 0)$$
$$= \frac{\omega}{4\pi\alpha}[\sigma_{pe}(\omega) - \sigma_{pc}(\omega)] . \quad (3.5)$$

The pair-creation cross section $\sigma_{pc}(\omega)$ noted here is not the usual atomic pair-production cross section, but corresponds to the process where the electron of the electron-position pair is created in the bound state of the given subshell.[41] No data are available on this bound-electron pair-creation process, although there are some theoretical predictions for the inverse process of one-photon pair annihilation with electrons of the K shell.[42,43] Since contributions to the imaginary part of the forward-scattering amplitude corresponding to $\sigma_{pe}(\omega)$ come only from the positive-energy perturbations $|n\kappa m_j +\rangle$ of the bound state, and contributions to $\sigma_{pc}(\omega)$ come only from the negative-energy perturbations $\langle n\kappa m_j -|$, it is possible for us to make separate predictions for $\sigma_{pe}(\omega)$ and $\sigma_{pc}(\omega)$.

B. Further verification of our Rayleigh amplitudes

Our predictions for the Rayleigh-scattering amplitudes are compared with several other available theoretical calculations. Although these comparisons serve mainly as a further verification of our numerical predictions, slight differences between amplitudes force us to discuss effects such as differences induced by the different choices in atomic-potential models. We found significant discrepancies in the 1.31-MeV calculations of Brown and Mayers[11] from our predictions at large angles.

1. Scofield's photoeffect cross sections

The photoeffect results of Scofield[44] can be directly used as a check of the imaginary parts of our forward-scattering amplitudes for energies below the bound-pair-production threshold. Scofield's photoeffect cross sections, tabulated for each subshell, were generated using DHFS wave functions with the Slater exchange potential. Table I displays sample comparisons by shell. Agreement is at the 1–2% level for all cases except for $Z=13$, where a difference of 7% exists for the L shell and 2–3% for the K shell. These differences may be attributed to the use of Slater vs Kohn-Sham exchange potentials. Both models are expected to account less accurately for exchange effects for light-Z atoms, and the difference in results will be larger for small Z. Ron and Tseng[45] found that for 5-keV photons on aluminum ($Z=13$), the difference between total photoeffect cross sections evaluated using the Slater exchange model and the Kohn-Sham exchange model ($\frac{2}{3}$ Slater's model) is 3.5% for the K shell and 7% for the L shell. This is very similar to the effect we found. For larger atomic numbers, the differences of photoeffect cross sections evaluated in these two different models are expect to be <2%.

2. Johnson and Cheng, 145-889 keV

In further tests of our calculations, we compared amplitudes generated by Johnson and Cheng[14] ($30 \leq Z \leq 82$, 145 keV $\leq \omega \leq$ 889 keV, K through M shells). Because of computer-code limitations, these authors did not make predictions for higher energies (which require continuum positron states) or lower energies. Since they employed the same realistic DHFS wave functions as we do, we expect good agreement in comparisons with our amplitudes. Johnson and Cheng reported the total differential Rayleigh-scattering amplitudes (summed over all shells included in their calculation) but only considered the lowest shells of the atom (in many cases only the K shell) which, however, usually dominate the scattering amplitudes for larger angles at these energies. For forward directions, where in fact many shells contribute, their results are incomplete for total-atom scattering, but they serve as an excellent check on our calculations of the same shells.

Table II compares five cases that Johnson and Cheng considered of the sum of the squared amplitudes. These represent extreme cases for the highest (Pb) and lowest (Zn) atomic numbers as well as the highest (889 keV) and lowest (145 keV)

TABLE I. Total photoeffect cross sections (in barns) obtained from the imaginary part of our forward-scattering amplitudes using the optical theorem are compared with the tabulation due to Scofield (Ref. 44). The larger differences for light Z are the result of the differing exchange potential models. (Scofield uses Slater, and we use Kohn-Sham.)

Z	ω (keV)	Shell	σ_{pe} (barns) Scofield	This work	% relative difference
13(Al)	8.04	K	2033.	1968.	3.3
		L	144.3	134.8	7.1
	59.5	K	4.097	4.012	2.1
	145.	K	0.2319	0.2246	3.3
47(Ag)	8.04	L	30820	30210	2.0
	59.5	K	859.7	852.7	0.8
		L	110.3	108.7	1.5
	145.	K	66.93	65.71	1.9
		L	8.109	7.920	2.4
	412.	K	3.524	3.501	0.7
	889.	K	0.5609	0.5567	0.8
82(Pb)	59.5	L	1193.	1182.	0.9
		M	282.0	278.2	1.4
	145.	K	544.7	541.2	0.6
		$L1$	58.16	57.28	1.5
		$L2$	24.04	23.48	2.4
		$L3$	20.60	20.12	2.4
		L	102.8	100.8	2.0
		M	24.09	23.56	2.3
	412.	K	36.98	36.83	0.4
		L	6.392	6.338	0.9
	889.	K	6.511	6.475	0.6
		L	1.077	1.066	1.0

TABLE II. The sum of squared scattering amplitudes (in r_0^2/sr) of Johnson and Cheng (denoted as JC, Ref. 14) are compared with the results of this calculation for the same shells. The agreement is excellent when the amplitudes are large. The number in parentheses indicates the associated power 10^n.

Z	ω (keV)	Shells included	θ (deg)	$\frac{1}{2}(\|A_{\|}\|^2+\|A_{\perp}\|^2)$ JC	This work	% relative difference
30	279	K	0	3.869	3.870	−0.03
			30	0.805 7	0.796 4	1.2
			60	0.052 26	0.051 12	2.2
			90	0.006 74	0.006 58	2.4
			120	0.002 72	0.002 65	2.6
			150	0.001 93	0.001 88	2.7
30	662	K	0	3.831	3.833	−0.05
			30	0.023 30	0.023 01	1.3
			60	1.60(−4)	1.63(−4)	−1.9
			90	1.24(−5)	1.34(−5)	−8.1
			120	5.11(−6)	5.97(−6)	−14.
			150	3.45(−6)	4.10(−6)	−19.
82	145	$K+L+M$	0	750.6	750.9	−0.04
			30	71.05	70.84	0.30
			60	11.34	11.20	1.2
			90	4.133	4.048	2.1
			120	2.974	2.911	2.2
			150	2.993	2.934	2.0
82	412	$K+L$	0	90.20	90.28	−0.10
			30	4.000	3.964	0.92
			60	0.433 5	0.432 2	0.30
			90	0.184 4	0.183 7	0.02
			120	0.146 8	0.146 1	0.50
			150	0.138 2	0.137 5	0.51
82	889	$K+L$	0	88.44	88.55	−0.12
			30	0.431 5	0.429 5	0.47
			60	0.240 9	0.023 90	0.79
			90	0.005 74	0.005 67	1.2
			120	0.003 67	0.003 64	1.4
			150	0.002 92	0.002 89	1.0

photon energies. These cases are also examples in which K, $K+L$, and $K+L+M$ shells of the atom were considered.[46] We observed generally excellent agreement (better than 0.1%) in the forward direction where the amplitudes are large. As would be expected, the relative error increases as the scattering angle increases. For forward directions, the multipole amplitudes (which are independent of angle) are summed with factors of the same sign; while at larger angles, they are added with factors of varying signs. The multipoles are generally of the same sign, so that the interference in the sum increases as the scattering angle increases, and a given error in multipole amplitudes leads to a larger error in the sum at larger angles. The error remains $O(1\%)$ whenever the summed amplitudes are large.

It should also be mentioned that in their calculations Johnson and Cheng have used the Slater exchange potential while, as noted earlier, we have used the Kohn-Sham ($\frac{2}{3}$ Slater exchange term). At these energies, the small differences between these two potential models are expected to generate differences at the 1% level, as were seen in the comparison earlier with Scofield's photoeffect cross sections.

We believe the good agreement in these five cases establishes the validity of our calculation in this energy range. We compare our predictions in this energy range with experiments in Sec. V.

3. Brown and Mayers, 1.31 MeV

Table III compares our results with those of Brown and Mayers[11] for 1.31-MeV photons scattered by the K shell of mercury in the Coulomb potential. We observe good agreement in the forward direction for the real parts and excellent agreement for the imaginary parts of the scattering amplitudes. But at intermediate and large angles large differences are found, especially in

TABLE III. The amplitudes (in classical election radii r_0) for 1.31-keV photons scattered by the K shell of mercury predicted by Brown and Mayers (denoted as BM, Ref. 11) are compared with our numerical calculation as a function of scattering angle (in degrees). Note the comparison of the sum of squared amplitudes (in r_0^2/sr) in the last three columns where small discrepancies in the forward direction increase with increasing angle. The amplitudes are complex and are listed as (Re, Im).

θ (deg)	$A_\parallel$ (Re, Im) BM	$A_\parallel$ (Re, Im) This work	$A_\perp$ (Re, Im) BM	$A_\perp$ (Re, Im) This work	$\frac{1}{2}(\|A_\parallel\|^2+\|A_\perp\|^2)$ BM	$\frac{1}{2}(\|A_\parallel\|^2+\|A_\perp\|^2)$ This work	% relative difference
0	−1.6989, 0.0474	−1.7365, 0.0475	−1.6989,0.0474	−1.7365,0.0475	2.889	3.018	−4.3
30	−0.2531, 0.0055	−0.2607, 0.0057	−0.3279,0.0211	−0.3330,0.0208	0.086 0	0.089 7	−4.1
60	0.0160, 0.0019	0.0049, 0.0020	−0.0426,0.0121	−0.0474,0.0119	0.001 11	0.001 21	−8.3
90	0.0295, 0.0015	0.0186, 0.0017	−0.0171,0.0073	−0.0176,0.0074	0.000 609	0.000 355	72
120	0.0253,−0.0001	0.0151, 0.0001	−0.0177,0.0047	−0.0128,0.0042	0.000 488	0.000 204	140
150	0.0228,−0.0015	0.0123,−0.0013	−0.0206,0.0029	−0.0177,0.0024	0.000 477	0.000 147	220
180	0.0206,−0.0023	0.0114,−0.0018	−0.0206,0.0023	−0.0114,0.0018	0.000 430	0.000 133	220

the real parts. To explain these differences we truncated the places of significance of our photon multipole amplitudes and compared the resulting sum of the squared scattering amplitudes. No gross change in the results occurs until our multipole amplitudes are truncated to 3 significant figures (see Table IV). The magnitude of the relative errors between 1 and 2 significant figures has an angular dependence similar to the discrepancies with Brown and Mayers. It is expected that approximately 1.5 places of significance (3%) are maintained in the amplitudes of at least the dipole terms of the Brown and Mayers calculation at 1.31 MeV.[47] At large angles, the destructive manner in which these multipole amplitudes combine to form the scattering amplitudes accounts for the observed factor-of-two discrepancy.

We studied this case because the theoretical elastic cross sections for energies 0.9–1.33 MeV showed large disagreements based on the amplitudes of Brown and Mayers. In Sec. V our prediction is consistent with experiment, and this provides additional support for the belief that the Brown and Mayers calculation is in error at back angles. Errors of this type do not affect the lower-energy calculations of Brown *et al.*, since the more rapid decay of the multipole contributions at lower energies reduces the severity of the destructive interference at large angles. In addition, the fundamental radial integrals have less rapidly oscillating integrands at lower energies, again reducing the difficulty of their accurate numerical evaluation.

4. Nonrelativistic Coulomb dipole for the K-shell

Further tests of our calculation are possible in the limiting cases corresponding to the nonrelativistic dipole approximation by Gavrila.[33] These are valid for light Z and low energies as long as screening effects are neglected. Table V compares Gavrila's amplitudes with our numerical dipole amplitudes obtained using both Coulomb and

TABLE IV. The sum of the squared scattering amplitudes (in r_0^2/sr) for 1.31- MeV photons scattered by the K shell of mercury are compared as a function of the scattering angle (in degrees). The amplitudes due to Brown and Mayers (denoted as BM, Ref. 11) are compared with amplitudes obtained from our numerically calculated multipole amplitudes that have been truncated to 3, 2, and 1 places of significance (denoted as KP3, KP2, and KP1, respectively). It is between 2 and 1 places of accuracy (3%) that our truncated amplitudes develop errors (as compared with our untruncated amplitudes) which have an angular distribution similar to the discrepancies of Brown and Mayers.

θ (deg)	$\frac{1}{2}(\|A_\parallel\|^2+\|A_\perp\|^2)$ BM	KP3	KP2	KP1	% relative difference BM	KP3	KP2	KP1
0	2.889	3.008	2.932	3.018	−4.2	−0.3	−2.9	0.0
30	0.086 0	0.089 5	0.088 1	0.081 5	−4.1	−0.2	−1.8	−9.1
60	0.001 11	0.001 22	0.001 20	0.002 09	−8.3	0.8	−0.8	72.
90	0.000 61	0.000 35	0.000 32	0.000 52	69.	−2.8	−11.	44.
120	0.000 49	0.000 21	0.000 26	0.000 71	145	5.0	30.	255
150	0.000 48	0.000 14	0.000 10	0.000 58	220	−6.7	−33.	287
180	0.000 43	0.000 13	0.000 26	0.001 42	230	0.0	100	992

TABLE V. Comparison of K-shell electric dipole Rayleigh-scattering matrix elements M (in r_0) for the nonrelativistic Coulomb case (denoted as NRC, due to Gavrila, Ref. 33), the relativistic Coulomb case (denoted as RC, this work), and the relativistic screened case (denoted as RS, this work).

			M electric-dipole matrix elements (Re, Im)			% relative difference (Re, Im)	
Z	ω (keV)	k (ω/Z^2 Ry)	NRC	RC	RS	NRC vs RC	NRC vs RS
13	5.41	2.35	−2.364, 0.5366		−2.277, 0.4731		3.8, 13.
	8.04	3.50	−2.237, 0.2494	−2.169, 0.2459	−2.136, 0.2222	3.2, 1.4	4.7, 12.
	22.1	9.61	−2.055, 0.0315	−1.700, 0.0297	−1.668, 0.0274	21. , 6.1	23. , 15.
	59.5	25.9	−2.010, 0.0036	−0.834, 0.0031	−0.797, 0.0028	140 , 16.	150 , 29.
47	8.04	0.268	0.180, 0.0000		0.172, 0.0000		5.0, 0.0
	59.5	1.98	−2.415, 0.7389	−2.057, 0.6780	−2.036, 0.6498	17. , 9.0	19. , 14.
	145.0	4.82	−2.156, 0.1319	−1.246, 0.0967	−1.230, 0.0936	73. , 36.	75. , 41.
	412.0	13.7	−2.031, 0.0147	−0.343, 0.0069	0.337, 0.0067	490 , 110	500 , 120
	889.0	29.6	−2.008, 0.0026	−0.090, 0.0013	0.088, 0.0013	2100 , 100	2200 , 100
82	22.1	0.242	0.144, 0.0000		0.096, 0.0000		49. , 0.0
	59.5	0.650	3.021, 0.0000	1.254, 0.0000	1.452, 0.0000	140 , 0.0	110 , 0.0
	145.0	1.59	−2.453, 1.101	−1.677, 0.9525	−1.666, 0.9212	46. , 16.	47. , 20.
	412.0	4.50	−2.171, 0.1514	−0.736, 0.0881	−0.729, 0.0862	190 , 72.	200 , 76.
	889.0	9.72	−2.054, 0.0367	−0.233, 0.0180	−0.230, 0.0177	780 , 100	790 , 110

screened (DHFS) potentials. We have mostly chosen cases where, numerically, the electric-dipole approximation holds, in the sense that the magnetic-dipole and electric-quadrupole amplitudes are typically smaller than the electric-dipole amplitude by an order of magnitude or more. The Rayleigh-scattering amplitudes for scattering of linearly polarized photons are expressed in terms of the electric-dipole matrix element M as

$$A_{\perp}^{R}(\omega,\theta)=M\,,\qquad A_{\parallel}^{R}(\omega,\theta)=M\cos\theta\,. \tag{3.6a}$$

We note the following features: (1) We find good agreement for light Z at 5 and 8 keV (this is a confirmation of our calculation at low energy) and fair agreement for intermediate Z below 59 keV. (2) The screening effects are of the same absolute magnitude in the real and imaginary parts, large for high Z near K-shell binding. Usefulness of these nonrelativistic Coulomb dipole results is restricted to light- and intermediate-Z elements for photon energies not more than several times the K-shell binding energy. For photon energies above 20 keV for aluminum, multipole effects are important. (See discussion of photon multipoles later in this section.)

C. Validity of the form-factor approximation, modified form-factor approximation, anomalous-dispersion corrections to the form factor, and the high-energy-limit formulas

With increased confidence in our numerical prediction of the Rayleigh-scattering amplitudes, we establish over what regions of (Z,ω,θ) parameter space several important approximations are valid. We concentrate primarily on the form-factor approximation and variations or corrections to it.

1. Form-factor approximation

We expect the form-factor approximation for scattering from a filled atomic subshell to be valid for light-Z elements at small momentum transfers q, and energies above and not too near the photoeffect threshold for that subshell. Figures 4–6 display the results of comparisons of the percent relative difference (in order to highlight differences) between the sum of squared amplitudes

$$\Sigma=\tfrac{1}{2}(|A_{\parallel}^{R}|^2+|A_{\perp}^{R}|^2) \tag{3.6b}$$

predicted by the form-factor approximation and those predicted by our numerical calculation summed over all electrons in the specific shell. The prediction in the form-factor approximation (in r_0^2/sr) is

$$\Sigma^{\mathrm{FF}}=\tfrac{1}{2}(1+\cos^2\theta)|f(q)|^2\,, \tag{3.7}$$

with $f(q)$ defined by Eq. (2.1). We calculated $f(q)$ using the single-particle electron number densities derived from the Dirac-Hartree-Fock-Slater (DHFS) wave functions used in our numerical calculation of the corresponding Rayleigh amplitudes $A_{\parallel}^{R}$ and $A_{\perp}^{R}$. The form-factor predictions are not compared with our numerical amplitudes for photon energies less than the electron binding energy of the subshell, since in this low-energy region the numerical amplitudes often change sign and bear no resemblance to the form-factor predic-

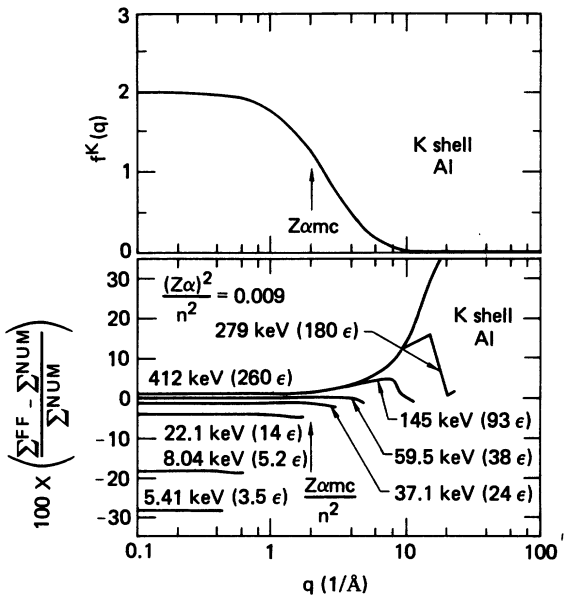

FIG. 4. The lower frame plots the percent relative difference between the sum of squared amplitudes predicted in form-factor approximation Σ^{FF} with predictions from our numerical evaluation of the second-order S matrix Σ^{NUM} as a function of momentum transfer for the K shell of aluminum. The upper frame plots the form factor for the K shell of aluminum f^K.

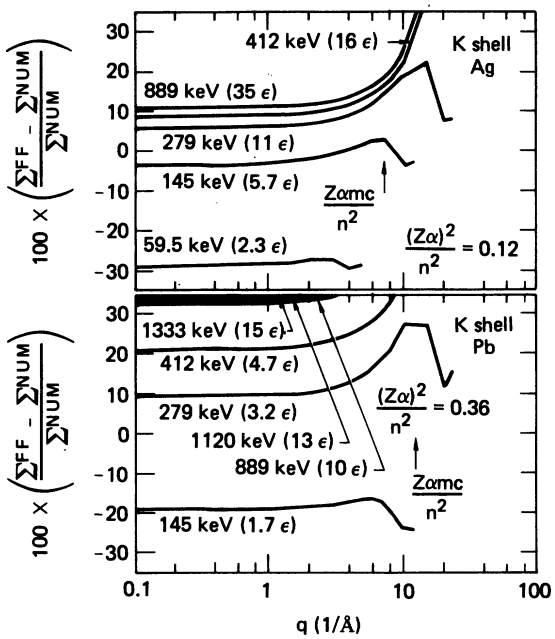

FIG. 5. The percent relative difference between Σ^{FF} and Σ^{NUM} for the K shell of silver and lead as a function of momentum transfer.

tions. Further, we restrict the comparison to photon energies above K-shell binding because the change in character of the exact single-particle K-shell amplitudes (being dominated by bound-bound-type transitions for $\omega<\epsilon_K$) affects all the atomic shells.[48] Figure 4 displays the form factor for the K shell of aluminum ($Z=13$) directly above the first comparison to remind the reader of the behavior of the K-shell form factor as a function of the momentum transfer q, and to emphasize that the deviation of Σ from constant difference is occurring at a momentum transfer that in general is different from q_{typ}, estimated by the inverse Bohr radius as $q_{typ}\simeq Z\alpha mc/n^2$.

Our numerical data in Figs. 4–6 indicate that, as in the form-factor approximation, the magnitude of the sum of the square numerical scattering amplitudes Σ of a given subshell is approximately constant for momentum transfers less than the typical momentum q_{typ} of electrons in that shell. (The constant is energy dependent.) This is physically plausible if we argue that the electron must largely supply this momentum. If the electron can make such a transition in momentum space and still finds itself within the bulk of the momentum distribution of this subshell, then the process should have a high probability, independent of q for $q\ll q_{typ}$. When the momentum transfer has increased beyond the typical momentum of electrons for this subshell, it will become increasingly improbable that the electron may elastically scatter the photon. This is consistent with the form-factor-approximation prediction. Note the relative error of the form-

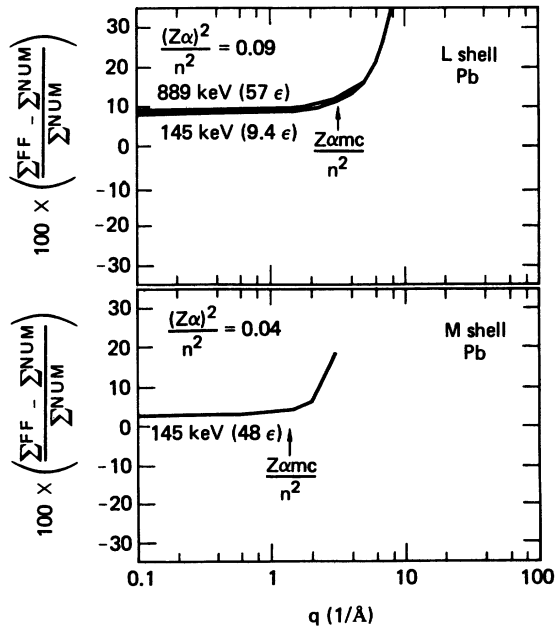

FIG. 6. The percent relative difference between Σ^{FF} and Σ^{NUM} for the L shell and M shell of lead as a function of momentum transfer.

factor prediction remains relatively constant even for q beyond q_{typ} for inner electrons of light-Z atoms. This relatively constant relative error extends until 0.1 or $0.2mc$ (2–4 Å^{-1}) for all Z, which for lightly bound electrons is into the region where the scattering amplitudes for these shells are decreasing rapidly. At momentum transfers greater than $0.2mc$ the form-factor approximation fails to decrease as rapidly as our numerical results. Thus, as a function of momentum transfer, the form-factor predictions for a filled shell fail universally as the magnitude of the momentum transfer approaches mc. This is consistent with Bethe's[21] derivation of the form factor where he assumed that $q \ll mc$.

We also note that Figs. 4–6 indicate the convergence of our numerical amplitudes at small q to a high-energy limit [since $f(q)$ is independent of ω]. The rate of convergence of the scattering amplitudes of a given shell to its high-energy limit is not strongly dependent on Z when considered as a function of ω/ϵ. Convergence of the amplitudes to the high-energy limit is achieved within 10% at 5ϵ, 5% at 10ϵ, and 1% at 20ϵ. This high-energy limit is close to the form-factor prediction for low Z, but smaller for high Z; the relative difference is of the order of $(Z\alpha/n)^2$. Bethe's derivation of the form factor uses the plane waves of the Born approximation for the intermediate states $|p\rangle$ of Eq. (3.1) and thus neglects corrections of order $(Z\alpha)^2$. For large momentum transfers at high energies, the form-factor approximation gives predictions that are grossly in error, often by factors exceeding 2–10. Yet, often the ratios of contributions are well predicted and the form-factor prediction that s waves (and particularly K-shell amplitudes) dominate is confirmed [see Eq. (2.8)]. We shall exploit these features in developing a prescription for simplified calculation of the total-atom amplitudes. (See relative contribution of shells discussion later in this section.)

Use of the form-factor approximation to predict differential (in scattering angle) elastic-photon-scattering amplitudes has the following validity as a function of atomic number, photon energy, and atomic shell. For photon energy above the K-shell binding energy ϵ_K for light atoms ($Z \sim 13$), predictions for the differential K-shell amplitudes for momentum transfers less than $0.2mc$ (4 Å^{-1}) are accurate to ~10% at $5\epsilon_K$ (7.5 keV for Al), 5% at $10\epsilon_K$ (15 keV for Al), and 1% at $20\epsilon_K$ (30 keV for Al). Large errors appear in the differential scattering cross sections predicted by the form-factor approximation for larger momentum transfers (scattering 90-keV photons through 90° corresponds to a momentum transfer of $0.2mc$). For all higher shells, the form factor predicts excellent differential amplitudes for photon energies greater than ϵ_K (1.5 keV for Al) and momentum transfers less than $0.2mc$. The smaller errors in predictions of the form factor for the higher shells will increase as decreasing photon energy approaches K-shell binding. Thus, the form factor will predict total-atom differential scattering cross sections accurate to at worst $O(2/Z)$ for energies greater than ϵ_K and forward angles.

For heavy atoms ($Z \sim 82$), there exists no energy region for which the K shell is accurately predicted by the form-factor approximation. The $(Z\alpha)^2$ heavy-atom corrections were neglected. For the K shell, errors in the differential amplitudes at high energies are still 15–20% for $q < 0.2mc$ and are bigger at larger momentum transfers. Errors in the differential L-shell amplitudes are smaller (5–10%) for photon energies greater than ϵ_K for small momentum transfers, while for the M shell errors in the differential amplitudes are less than 5% for $\omega > \epsilon_K$ and small q. Thus, for total-atom differential cross sections, errors of the order 5–15% are expected for forward angles and $\omega > \epsilon_K$ (90 keV for Pb) with big errors at larger momentum transfers.

These observations have direct implications for the total-atom (summed over electrons) total cross section (integrated over angles) defined as

$$\sigma(\omega) = \int \frac{d\sigma}{d\Omega} d\Omega = \frac{2\pi}{\omega^2} \int_0^{2\omega} \frac{d\sigma}{d\Omega} q\, dq . \tag{3.8}$$

Here $d\sigma/d\Omega$ is the total-atom cross-section differential in angle given, for unpolarized incident radiation when final polarizations are not measured, by

$$\frac{d\sigma}{d\Omega} = \frac{r_e^2}{2}\left(\left| \sum_e A_{\parallel}^R \right|^2 + \left| \sum_e A_{\perp}^R \right|^2 \right). \tag{3.9}$$

The symbol $\sum_e$ denotes the sum over all bound electrons. Since the contribution to this total cross section from a given electron decreases rapidly for momentum transfer greater than q_{typ}, errors made by the form-factor approximation for this electron for higher momentum transfers will not strongly affect the total cross section. The contribution of a given electron to the total-atom total cross section will be correctly accounted for in the form-factor approximation if the form factor correctly predicts the differential amplitudes for the electron for momentum transfers up to q_{typ}. This is the case for all shells of low-Z elements at high energies, and similarly for high Z except for the K shell (i.e., for $\epsilon \ll mc^2$ and $\omega \gg \epsilon$). We compare our prediction of total-atom total cross sections with those of form factor in Sec. IV.

2. *Modified form-factor approximation*

We have noted that in his derivation of the form-factor approximation, Franz[20] suggests an improvement, resulting in the modified form factor $g^i(q)$. [See Eq. (2.9).] Comparisons of the sum of squared amplitudes given by Eq. (3.7) with $f(q)$ replaced by $g(q)$, with our numerical amplitudes are shown in Figs. 7 and 8. There is indeed a considerable improvement over the form-factor approximation: (1) in extending the range of momentum transfers for which the form-factor approximation is valid ($0<q<0.5mc$ for the K shell independent of Z); and (2) for high Z (the magnitude of the error becomes small in the high-energy limit for small momentum transfers independent of binding energy). The range of valid momentum transfers is sufficient to include major regions of even the K-shell distribution of heavy atoms.

For the K shell of light atoms, comparisons of our numerical results with the modified form factor (Fig. 7) and the ordinary form factor (Fig. 4) shows little difference for $q<0.1mc$ (2 Å^{-1}), but the modified form factor continues to provide good predictions for momentum transfers up to $0.5mc$ (10 Å^{-1}). At this higher momentum transfer, the sum of squared K-shell scattering amplitudes (which heavily dominate the total-atom scattering amplitudes at this q) is down by more than a factor of 1000 as compared with its value at $q=0$. Errors in the K-shell amplitudes of light-Z elements predicted by the modified form factor are at the 10% level by about $5\epsilon_K$, the 5% level by about $10\epsilon_K$, and the 1% level by about $25\epsilon_K$. For the K shell of medium and heavy atoms, the prediction of the modified form factor at finite energies is a major improvement over the ordinary form factor, and this improved agreement also extends to the higher momentum transfer of $0.5mc$. Errors in the K-shell amplitudes of heavy-Z elements predicted by the modified form factor are at the 10% level by about $3\epsilon_K$, the 5% level by about $5\epsilon_K$, and the 1% level by about $10\epsilon_K$. Improved agreement over the form factor is also found in predictions of the modified form factors for higher shells for $\omega \gtrsim \epsilon_K$. The range of valid momentum transfers, although less than that for the K shell, is sufficient to include the regions where the contributions to the total-atom differential amplitudes are large (i.e., $q \lesssim q_{\text{typ}}$).

Thus, accurate total-atom differential scattering amplitudes may be calculated using the modified form-factor approximation for all shells of all atoms for forward angles and photon energies greater than K-shell binding. The errors in the resulting total-atom differential scattering amplitudes for light-Z atoms will be less than 10% at about $5\epsilon_K$, 5% at about $10\epsilon_K$, 1% at about $25\epsilon_K$.

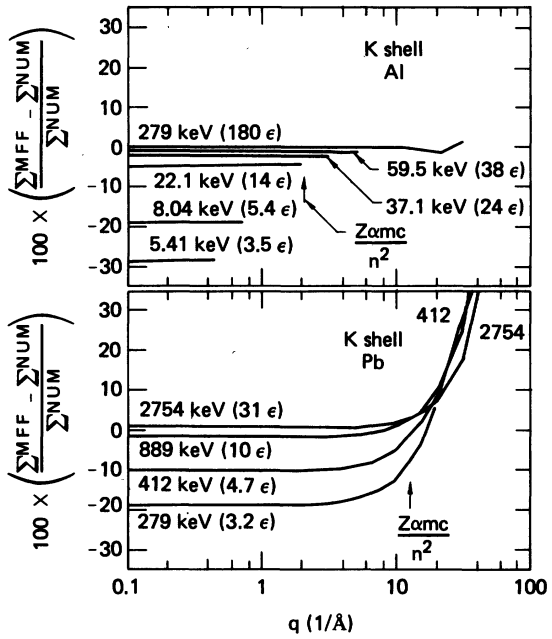

FIG. 7. The percent relative difference between the sum of squared amplitudes predicted in the modified form-factor approximation Σ^{MFF} and predictions from our numerical evaluation of the second-order S matrix Σ^{NUM} as a function of momentum transfer for the K shell of aluminum and lead.

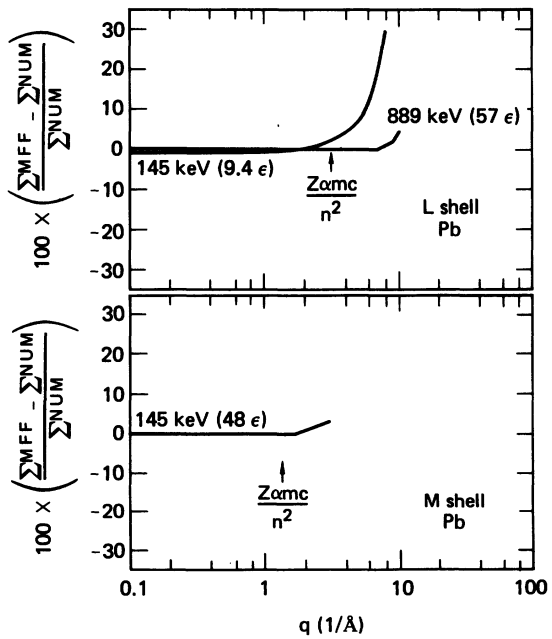

FIG. 8. The percent relative difference between Σ^{MFF} and Σ^{NUM} for the L shell and M shell of lead as a function of momentum transfer.

The errors in the resulting total-atom differential scattering amplitudes for heavy-Z atoms will be less than 1% at about $3\epsilon_K$ because of the larger number of outer electrons.

3. *High-energy limit for the K-shell*

Florescu and Gavrila[32] have recently derived analytic expressions for the Rayleigh K-shell scattering amplitudes in the Coulomb potential in the limit of high photon energy ($\omega \to \infty$) and finite momentum transfer,[49] extending the near $\theta = 0$ results of Goldberger and Low.[31] Figure 9 compares the sum of squared amplitudes of our numerical calculation Σ^{NUM} using Coulomb wave functions, with their high-energy matrix element Σ^{HE}. The deviation of the high-energy-limit amplitude from our finite-energy numerical calculation remains relatively independent of momentum transfer for momentum transfers small as compared with $2\omega m c$. This region of constant fractional difference of the high-energy-limit amplitude from our numerical results encompasses larger momentum transfers as photon energy increases. Figure 9 illustrates the agreement with the high-energy-limit results extends well beyond the region where the aluminum K-shell amplitudes are large. This suggests valid use of the high-energy limit for prediction of the total (integrated differential) cross section at sufficiently high photon energy. Also the differences between Σ^{HE} and Σ^{NUM} are 10–20% for photon energy $5\epsilon_K$, 4–6% for photon energy $10\epsilon_K$, and less than 1% for photon energy greater than $20\epsilon_K$ (where ϵ_K is the K-shell binding energy). The rate of convergence of our numerical calculations to the high-energy-limit amplitude is similar to the rate of convergence of our numerical results to the predictions of the modified form factor for the K shell of heavy-Z elements using DHFS wave functions (Fig. 7), but the departures are in the opposite direction. At high photon energy the effects of screening on the K-shell scattering amplitudes are found to be small, and there would seem to be no preference between the use of the modified form-factor approximation and the high-energy-limit results for prediction of the K-shell Rayleigh-scattering amplitudes for smaller values of q. [Recall that at high photon energy, the Rayleigh amplitude is dominated by the K shell at ordinary angles ($\theta > 1°$).] However, the validity of the high-energy-limit amplitude is found to extend to larger values of q as ω increases.

4. *Effects of screening*

It is important to determine how screening of the nuclear charge by the bound electron affects the Rayleigh-scattering amplitudes for atomic electrons. This is needed both to understand physical effects which can result and to understand the appropriateness of various more approximate calculational schemes.

To anticipate the results, we recall that the form-factor approximation makes a prediction of these effects. Because the form factor has some approximate validity for photon energies greater than electron binding, qualitatively correct predictions concerning the effects of screening are expected for higher photon energies. The form-factor approximation predicts the following effects of screening for photon energies greater than electron binding: (1) For small momentum transfers, the form factor, Eq. (2.1), reduces to N, the number of electrons, which is independent of the type of atomic potential used. Thus, for high energy and small momentum transfers, no screening effects are predicted in the form-factor approximation. (2) For large momentum transfers, the form factor is Coulomb-like except for bound-state-normalization corrections, since the charge densities used are Coulomb-like for small distances except for normalization corrections.[50] So for high energy and large momentum transfer, the effect

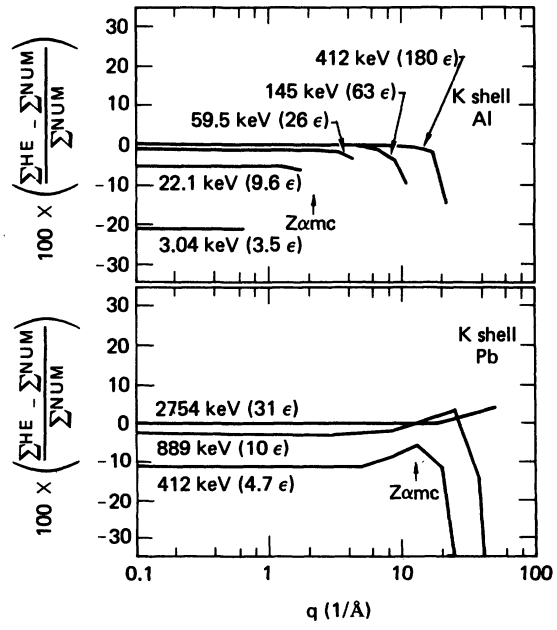

FIG. 9. The percent relative difference between the sum of squared amplitudes predicted using the high-energy-limit amplitude Σ^{HE} with predictions of our numerical evaluation of the second-order S matrix Σ^{NUM} as a function of momentum transfer for the K shell of aluminum and lead.

of screening in the scattering amplitudes may be expressed as the squared ratio of screened to unscreened bound-state normalizations (a constant independent of momentum transfer). (Since the form factor is not valid for large momentum transfer, we must examine our numerical data to see whether this prediction is in fact valid.)

Figure 10 compares the sum of squared amplitudes predicted using Coulomb wave functions with the same quantity predicted with screened DHFS wave functions. For photon energies greater than several times electron binding, there are essentially no screening effects on the total cross section (integrated over angle). For large momentum transfer, the ratio of squared normalizations predicts approximately a constant 15% screening effect for aluminum (we found a 19% effect) and a 3% effect for lead (we found a maximum 4% effect although the effect did not become momentum independent by the end of the comparisons). Thus, generalizing to other shells, we expect that for energies several times electron binding, screening effects are essentially zero for momentum transfers less than $Z\alpha mc/n^2$. These corrections increase in the neighborhood of $Z\alpha mc/n^2$ to an asymptotic value given by the ratios of squared bound-state normalizations (at least for light Z). So the form factor has correctly predicted screening corrections (at least when large) even when it does not predict the amplitudes well.

For photon energies in the neighborhood of or below electron binding, the form-factor approximation is no longer valid. Screening corrections, especially to the wave functions of outer bound-electron orbitals, will be large. Even for the inner shells, the position of the edge is shifted. Figure 10 shows that the comparison of our screened and unscreened numerical calculations differ strongly for the case of 59.5-keV photons on lead (K-shell binding energy is 88 keV). Screening effects in the Rayleigh amplitudes are important for all Z just above threshold because the Re and Im parts of the amplitudes are comparable. As was shown earlier, the Im part of the forward-scattering amplitude is related to photoeffect, which is sensitive to screening near threshold.

We may also review Table V, in which we compare screened and unscreened dipole matrix elements for the K shell. We again find that screening effects are small in the dipole matrix elements for photon energies much greater than ϵ_K. In the regime where the dipole amplitude is sufficient to describe the differential amplitudes, screening effects will be a constant factor independent of momentum transfer. This constant factor will also be reflected in the total cross sections (integrated over angles).

5. Relative contribution of shells

Figures 11–13 plot the ratio of the sum of squared amplitudes of a higher shell $\Sigma^{\rm NUM}_{{\rm DHFS}-i}$ to that for the K shell $\Sigma^{\rm NUM}_{{\rm DHFS}-K}$ as a function of momentum transfer q for photon energy greater than K-shell binding. Instead of showing the two complex amplitudes, we compare the sum of squared amplitudes to simplify the comparison although photon polarization information is lost. In the form-factor approximation, the quantity we display reduces to the ratio of the squares of the higher-shell form factor to the K-shell form factor. This quantity is a universal function of q, independent of photon energy, for fixed Z in the form-factor approximation.

For small q these ratios are close to the square of the relative number of electrons in the shell. These ratios decrease rapidly in magnitude for intermediate values of q but level off for very large q. For large q, the constant value reflects the contribution of bound electrons with orbital angular momentum $l=0$ (s waves). (See previous discussion of form factors.)

Comparing our numerical amplitudes with the form factor and modified form factors, we find that these approximate theories are not valid at large q even for large photon energy. The modified form factor itself fails for $q \geq 10$ Å^{-1}, while the form factor fails for even smaller q. In some intermediate- and large-q situations, the ratios

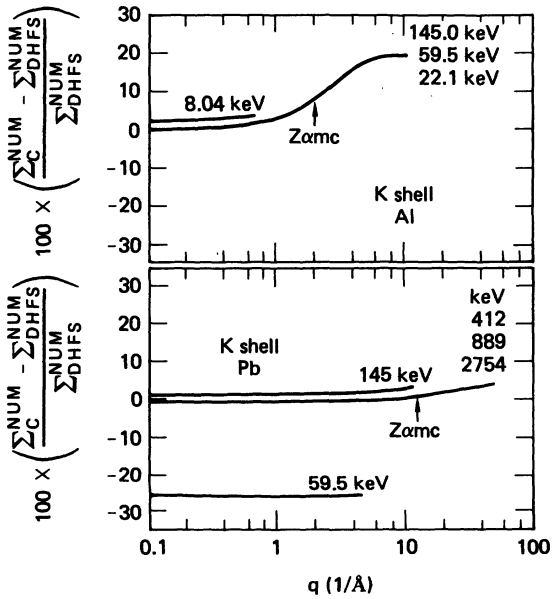

FIG. 10. The percent relative difference between the sum of squared amplitudes predicted using Coulomb wave functions $\Sigma^{\rm NUM}_{C}$ with our predictions using DHFS wave functions $\Sigma^{\rm NUM}_{\rm DHFS}$ as a function of momentum transfer.

of shells will be well estimated as ratios of form factors or modified form factors even when the form factor or modified form factor itself is not valid. As noted earlier, such form-factor or modified-form-factor ratios are useful at photon energies several times K binding since there are q independent errors in these approximate theories closer to threshold. At higher energies both ratios work well and differ little for low Z. For high Z, the modified form factor is a distinct improvement through small and intermediate q since it correctly includes corrections in $(Z\alpha/n)^2$; however, changes in sign found in our modified form factors at large q for large atomic numbers limit the usefulness of ratios in this region.

We observe from the example of Figs. 11–13 that the ratios of both the form factor and modified form factor, although qualitatively correct, are not accurate in the region of rapid variation of our numerical ratios for intermediate values of q. But, since the numerical ratios are small in this region, either the form-factor or modified-form-factor ratios may be used to estimate the contribution of higher shells to the total-atom differential scattering amplitudes. At very large momentum transfers where the numerical ratios are expected to be less rapidly changing, we expect the form-factor ratios to represent more uniformly the numerical ratios. We conclude that using ratios of form factors to estimate the contribution of the outer atomic shells provides an estimate for large q.

6. *Importance of photon multipole and relativistic effects*

In our numerical calculation we truncate the photon multipole series [see Eq. (3.3)] when the relative magnitude of the real part of the Jth electric multipole amplitude (X_J^1) has dropped 5 orders of magnitude below the real part of the electric dipole amplitude (X_1^1). For cases that require less than 6 photon multipoles, the real part of the electric dipole amplitude (X_1^1) is typically an order of magnitude greater than the real part of the magnetic dipole amplitude (X_1^0) or the real part of the electric quadrupole amplitude (X_2^1). This relativistic dipole scattering region exists for photon energy $\omega > 10\epsilon^{1/2}$ (in keV). (It would seem possible that, near "forbidden" dipole resonant transitions like $1s \rightarrow 3s$, high multipole amplitudes could be more important than the dipole amplitude; but such cases have not been examined.) For photon energy $\omega > 10\epsilon^{1/2}$, higher-multipole effects become increasingly more important. Figure 14 displays the number of photon multipole amplitudes we found necessary to include for sample K-, L-, and M-shell calculations for aluminum ($Z = 13$)

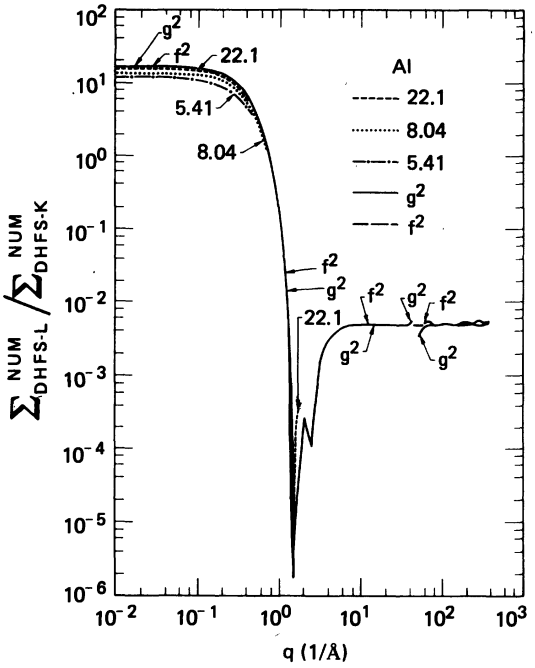

FIG. 11. We plot for several energies the ratio of the sum of squared amplitudes of the L shell Σ^{NUM}_{DHFS-L} to the K shell Σ^{NUM}_{DHFS-K} for aluminum, together with form-factor and modified form-factor predictions (labeled f^2 and g^2) as a function of momentum transfer.

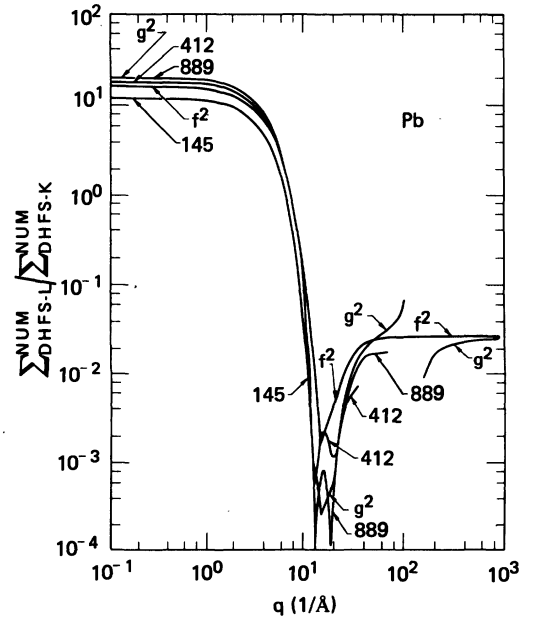

FIG. 12. We plot for several energies the ratio $\Sigma^{NUM}_{DHFS-L} / \Sigma^{NUM}_{DHFS-K}$ for lead as a function of momentum transfer, as in Fig. 11.

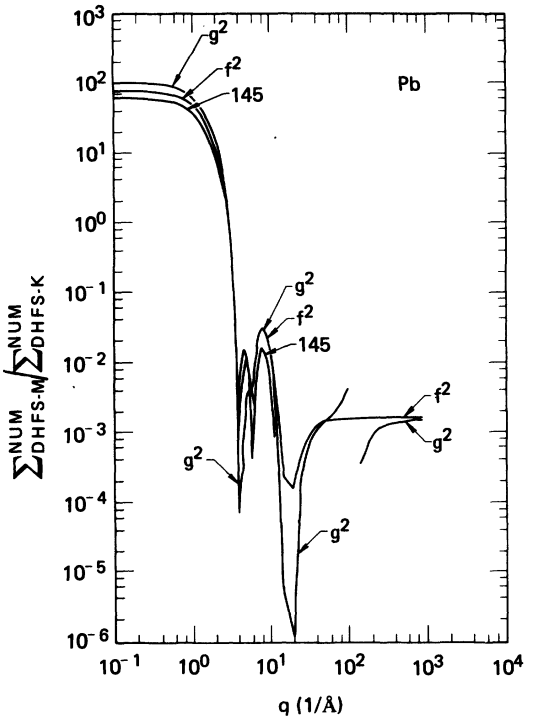

FIG. 13. We plot for several energies the ratio $\Sigma^{NUM}_{DHFS-M}/\Sigma^{NUM}_{DHFS-K}$ for lead as a function of momentum transfer, as in Fig. 11.

and lead ($Z=82$) for photon energies greater than K-shell binding. The number of multipoles required to satisfy our convergence criteria is essentially a universal curve that depends on photon energy relative to the square root of the electron's binding energy.

From the comparison of our numerical amplitudes with the nonrelativistic dipole K-shell amplitudes of Gavrila,[33] we estimate the importance of relativistic effects on the Rayleigh-scattering electric-dipole amplitude. (See discussion earlier in this section and Table V.) The relativistic effects for light atoms ($Z=13$) for energies above but near K-shell binding are small. As the photon energy continues to increase above K-shell binding, relativistic effects become increasingly more important for all atomic numbers, but especially for heavy elements. [Recall that higher-multipole effects become important at about 20 keV for aluminum ($Z=13$), and at about 150 keV for lead ($Z=82$).] More investigation is required for photon energies below K-shell binding.

IV. ACCURATE DIFFERENTIAL AND TOTAL RAYLEIGH CROSS SECTIONS

In this section we discuss our prescription for obtaining predictions of the Rayleigh-scattering amplitudes necessary for accurate [error $O(1\%)$] differential and total cross sections. We tabulate representative samples of the amplitudes so obtained and discuss their properties. From the comparisons of our numerical results with theory in Sec. III, we can accurately predict the differential scattering amplitudes for isolated atoms via our numerical evaluation of the second-order S matrix within the energy range 100 eV–10 MeV. This energy range includes energies as low as we expect our results to be qualitatively valid (because of increasing importance of electron correlations) and energies high enough to observe convergence to analytic high-energy results. Since this calculation requires substantial costly amounts of computer time—especially at higher energies for atoms with many electrons—we have sought methods for total-atom predictions tested by our numerical results that rely on simpler theories.

A. Prescription for accurate total Rayleigh amplitudes

In our comparisons of the predictions of other theories with our numerically evaluated S-matrix Rayleigh amplitudes, we found no simple theory that proved useful for predicting the inner subshell amplitudes over a wide range of Z, ω, and q. For the accurate prediction of inner-electron Rayleigh amplitudes at all values of Z, ω, and q in our region of interest, we must rely on amplitudes based upon our numerical evaluation of the second-order S matrix. Inner electrons are the electrons in those shells whose binding energy is not small compared with the photon energy or which contribute heavily to the total-atom differential cross section at large momentum transfers q.

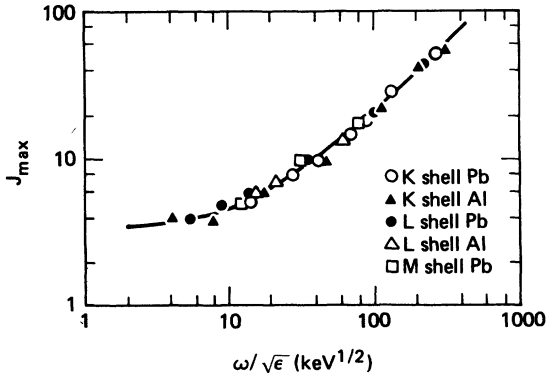

FIG. 14. The number of photon multipoles J_{max} required for convergence of our numerical evaluation of the second-order S matrix as a function of photon energy. Note: J_{max} is relatively independent of atomic shell or Z when plotted as a function of photon energy relative to the square root of the corresponding electron binding energy ϵ.

Outer electrons are the electrons in those shells whose binding energy is small compared with the photon energy and which contribute lightly to the total-atom differential cross section at large momentum transfers q. We could also, in principle, obtain accurate Rayleigh amplitudes via our numerical evaluation of the S matrix. This would be prohibitively time consuming for heavy atoms with many electrons, especially at large ω. For an alternative approach, we review the results of our comparisons with simpler theories. Possible candidates for models to estimate the contribution of outer electrons all rely strongly on some type of form-factor approximation. We have investigated[12] the use of the form-factor approximation $f(q)$, the modified form-factor approximation $g(q)$, ratios of either the form factors or modified form factors to scale from the numerical inner-electron amplitudes, photoeffect cross sections and the optical theorem, and the suggestion of Brown and Mayers in which $g(q)$ is used to estimate the no-spin-flip amplitude A_{NSF} while $f(q)$ is used to estimate the spin-flip amplitude A_{SF}.

We may specify our prescription for accurate Rayleigh-scattering amplitudes for photon energies ω above K-shell binding. For the inner electrons, we will use amplitudes derived from our numerical evaluation of the second-order S matrix. For outer electrons, we will estimate their contribution to the real part of the Rayleigh amplitudes using the modified form-factor approximation for $q < 50$ Å^{-1}. The expression for the contribution to the real part of the Rayleigh amplitudes in the modified form-factor approximation is similar to that in the form-factor approximation, Eq. (2.2), but one replaces the form factor $f^i(q)$, Eq. (2.1) by the modified form factor $g^i(q)$, Eq. (2.9). We use the forward-angle ratio of outer-electron to inner-electron imaginary amplitudes predicted by the optical theorem equation (3.4) and the photoeffect cross sections of Scofield[44] to scale the inner-electron imaginary amplitudes at all angles. For $q > 50$ Å^{-1}, the contribution of the outer electrons to the real total-atom Rayleigh amplitudes is estimated using the ratio of the outer-electron form factor to the K-shell form factor to scale the real part of the numerical S-matrix amplitude for the K shell. (At very high energies, one could substitute the high-energy-limit amplitude of Florescu and Gavrila[32] for our numerical S-matrix amplitude for the K shell.) For ^{82}Pb, we estimate that for $\omega > 889$ keV, use of the K-shell S-matrix amplitudes with remaining electrons being approximated as above gives Rayleigh amplitudes accurate to $O(2\%)$.

For photon energies below the photoeffect K edge, progressively more of the outer electrons must be included via the numerical S matrix as the photon energy decreases. There are two reasons for this: (1) the modified form factor becomes a poorer approximation for a particular bound electron as the photon energy approaches the photoeffect threshold for ejection of that electron, and (2) use of the modified form-factor approximation to estimate the contributions from outer electrons neglects transitions to inner-electron orbitals which are included in the detailed formalism used in our numerical calculation of the S matrix. These contributions [coming from the evaluation of the Furry diagram where the scattered photon is emitted first, Fig. 3(b)] are needed to cancel

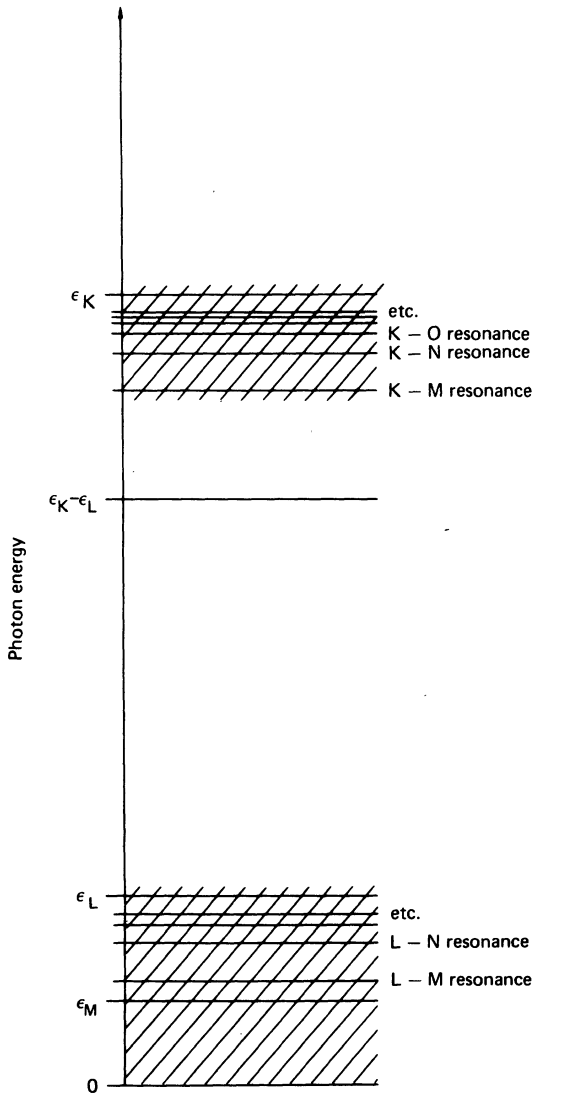

FIG. 15. Regions of photon-energy space where a direct numerical calculation of the K- and L-shell Rayleigh amplitudes using modified form factors to estimate the contribution of all higher shells would be unsafe.

complementary transitions included in our numerical calculation of the inner electrons using the second-order S-matrix formalism. These resonant transitions become large when the photon energy approaches the difference between any two bound energy levels. Thus, use of the modified form-factor approximation to estimate the contribution from a particular outer electron is restricted to energies greater than several times electron binding and photon energies not too near the resonance energies connecting this electron orbital with an inner-electron orbital which has been calculated directly using the numerical S-matrix method. This complication of the prescription for energies below the photoeffect K edge is due to our mixing of two formalisms in an effort to minimize the computational time. If the entire atom (24 subshells for lead) is calculated within the numerical S-matrix formalism, this complication does not arise, since the cancellation of these false resonant transitions occurs automatically when the final sum over all occupied orbitals of the atom is performed. Real resonant transitions between, for example, the K shell and unoccupied excited states would, of course, remain. Assuming that K- and L-shell contributions to the Rayleigh-scattering amplitudes are calculated using the S-matrix formalism and higher shells are estimated using the modified form-factor approximation, we display in Fig. 15 regions of photon frequency space where such a calculation is unsafe for a heavy element such as lead. Figure 15 shows photon energies for which uncanceled K- or L-shell-to-higher-subshell resonant contributions are large enough to distort the resulting Rayleigh-scattering amplitudes. Table VI lists values of the electric and magnetic dipole amplitudes for the K shell of lead for photon energies below and above the $K \rightarrow M \rightarrow K$ resonance. The contributions to the Rayleigh-scattering amplitudes from these multipole amplitudes are

$$A_{\perp}^{R}(\omega,\theta) = -\tfrac{3}{2}(X_1^1 + X_1^0\cos\theta),$$
$$A_{\parallel}^{R}(\omega,\theta) = -\tfrac{3}{2}(X_1^0 + X_1^1\cos\theta), \tag{4.1}$$

where X_1^0 is the magnetic dipole and X_1^1 is the electric dipole X amplitude. We note the rapid rise and change of sign of the electric dipole amplitude as the photon energy passes through the $K \rightarrow M \rightarrow K$ resonance energy.

B. Sample tabulations for Pb and some general features exhibited by the total-atom Rayleigh amplitudes

Table VII, Fig. 16, and Fig. 17 present sample tabulations of total-atom elastic-photon-scattering amplitudes and cross sections of several photon energies in the range 10 keV–10 MeV for neutral lead ($Z = 82$). These data are the result of including the Rayleigh amplitudes for all 82 atomic electrons and the nuclear Thomson amplitudes. The nuclear Thomson (NT) amplitudes are given in units of r_0 by

$$A_{\perp}^{\mathrm{NT}} = -Z^2 m/M,$$
$$A_{\parallel}^{\mathrm{NT}} = A_{\perp}^{\mathrm{NT}}\cos\theta, \tag{4.2}$$

where m/M is the ratio of electron rest mass to the atomic mass, and $m/M \simeq 1/1823A$ where A is the atomic weight. Explicitly, for lead the nuclear Thomson amplitudes may be written as

$$A_{\perp}^{\mathrm{NT}}(\mathrm{Pb}) = -0.017\,80,$$
$$A_{\parallel}^{\mathrm{NT}}(\mathrm{Pb}) = -0.017\,80\cos\theta.$$

The total-atom Rayleigh amplitudes are evaluated using the prescription described earlier in this section. Table VIII shows how the 82 electrons of neutral lead have been divided between inner and outer electrons. Table VIII also lists the values of the photoeffect cross-section ratio used in estimating the imaginary Rayleigh amplitudes for outer electrons. As the photon energy decreases, more and more of the shells of larger principal quantum numbers are included in the class of inner electrons. In two cases ($\omega = 59.5$ and 279 keV), more electrons have been included in the class of inner electrons (since the more accurate numerical amplitudes were available) than our prescription for accuracy $O(1\%)$ would require. In some cases ($\omega = 1120$, 1170, and 2750 keV), fewer electrons have been included than are re-

TABLE VI. Values of the electric and magnetic dipole amplitudes (in classical electron radii) for the K shell of lead ($Z = 82$) for energies starting 2 keV below the $K \rightarrow M_I \rightarrow K$ resonance and ending 1.5 keV above the $K \rightarrow M_V \rightarrow K$ resonance. Resonance is expected for photon energies in the range 84–86 keV. Note the rapid rise (and change of sign) of the electric dipole amplitude as the energy approaches the $K \rightarrow M \rightarrow K$ resonance region.

ω (keV)	X_1^1 electric	X_1^0 magnetic
82.141	−0.2622	−0.024 19
82.641	0.1345	−0.023 98
83.141	0.6829	−0.023 36
83.641	1.634	−0.021 17
85.975	−1.885	−0.027 56
86.475	−0.7537	−0.026 87
86.975	1.280	−0.020 28

quired to maintain $O(1\%)$ accuracy. We estimate that in these cases larger $O(2\%)$ errors are present due to unavailability at this time of numerical S-matrix L-shell amplitudes.

We have ignored the contribution to the elastic-photon-scattering amplitudes and cross sections made by the nuclear-resonance and Delbrück-scattering processes. At higher energies, comparisons with experiment require the inclusion of the nuclear-resonance and Delbrück-scattering amplitudes.

We also collected data to perform a direct comparison with the anomalous scattering factors that were calculated relativistically by Cromer and Liberman.[30] These anomalous scattering factors are tabulated for photon energies of 5.41–22.1 keV for all neutral atoms of $Z<99$. Predictions by subshell in the same energy interval may be obtained using a program and data supplied by Cromer and Liberman in their Los Alamos Scientific Laboratory report, but a direct comparison with our predictions by subshell is not immediately possible, because Cromer and Liberman have analytically carried out the sum over all electrons for certain terms in their calculations.

Table IX compares forward-angle amplitudes derived from the anomalous scattering factors calculated by Cromer and Liberman (which utilize the photoeffect cross sections of Brysk and Zerby[51]) with our predictions. Agreement is good in all cases. It may be noted that we find a phase difference which yields imaginary forward-angle Rayleigh-scattering amplitudes which differ in sign from ours. We suggest that the phase convention adopted by Papatzacos[52] be used for all elastic-photon-scattering amplitudes. This phase convention becomes important when independently calculated elastic amplitudes are coherently added to predict elastic cross sections. This point is academic in the energy range considered by Cromer and Liberman since no other elastic amplitudes contribute significantly here.

Table X compares total-atom total cross sections, Eq. (3.8), predicted using our prescription with predictions of form-factor approximation for lead ($Z=82$). These total cross sections include only the contribution due to Rayleigh scattering and are not directly comparable with experiment for the higher photon energies considered in the comparison. In these heavy elements a region of validity below the K edge exists. We also note that the nonrelativistic form-factor cross sections better approximate our predictions than the corresponding relativistic form-factor values. The difference from form-factor approximation is largest for energies just below the photoeffect K edge (88 keV for Pb) for example 26% at 75 keV. Rayleigh scattering contributes 10%–20% to the total attenuation coefficients for photon energies immediately below the K edge of high-Z elements. Consequently, it would appear that predictions for attenuation coefficients, tabulated using the form-factor approximation for Rayleigh scattering, could be in error by several percent in this energy range. At other energies, scattering is no longer a significant process for attenuation. (On the other hand, these deviations of Rayleigh scattering off atomic electrons from form-factor behavior at low energies are crucial in explaining the response of the atom to electromagnetic radiation, as discussed by Johnson and Feiock[13] in their calculation of atomic susceptabilities.)

Using our sample tabulations, we may observe various qualitative features and properties of the elastic, and in particular the Rayleigh, scattering amplitudes. We first note that the amplitudes have the following symmetries which follow directly from Eqs. (3.3) and (4.2),

$$A_{\parallel}(\omega,\theta=0^\circ)=A_{\perp}(\omega,\theta=0^\circ),$$
$$A_{\parallel}(\omega,\theta=180^\circ)=-A_{\perp}(\omega,\theta=180^\circ). \tag{4.3}$$

These same symmetries are also found in the form-factor and modified form-factor approximations.

The qualitative energy, angle, momentum transfer, and Z dependence of the magnitude of the real parts of the Rayleigh amplitudes are seen to be form factorlike for energies well above the photoeffect edges. The magnitude of the real parts of the forward Rayleigh amplitudes are equal to 82 in the form-factor approximation. The magnitude of the real parts of our forward-Rayleigh amplitudes are found to be less than 82; this value tends

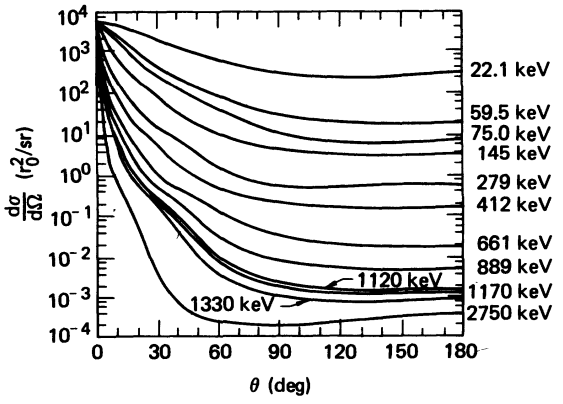

FIG. 16. The total-atom differential elastic-photon-scattering cross sections of Table VII as a function of scattering angle.

TABLE VII. Sample tabulations for lead ($Z = 82$) of the total-atom (summed over electrons) elastic-photon-scattering amplitudes at several photon energies in the range 10 keV–10 MeV. These data are the result of coherently summing the amplitudes due to Rayleigh (R) scattering and nuclear Thomson (NT) scattering. The effects due to Delbrück scattering and nuclear-resonance scattering have not been included. The data displayed by column from left to right are the photon energy ω in keV, the scattering angle θ in degrees, the real and imaginary parts of the parallel $A_{\parallel}$ and perpendicular $A_{\perp}$ scattering amplitudes in units of classical electron radii, the differential unpolarized elastic photon scattering cross section in barns/sr, and the total unpolarized elastic-photon-scattering cross section $\sigma(\omega)$ (integrated over angles) in barns.

		Elastic Amplitudes (R + NT) in r_0					
ω (keV)	θ (deg)	$\mathrm{Re}A_{\parallel}$	$\mathrm{Im}A_{\parallel}$	$\mathrm{Re}A_{\perp}$	$\mathrm{Im}A_{\perp}$	$\frac{d\sigma}{d\omega}$ (barn/sr)	$\sigma(\omega)$ (barns)
2750	0	−81.0	0.030 6	−81.0	0.030 6	521.	0.114
	10	− 0.683	0.013 9	− 0.699	0.019 3	0.037 9	
	30	− 0.035 5	0.003 65	− 0.0520	0.011 0	1.63(−4)	
	60	− 0.004 04	0.001 91	− 0.0195	0.006 44	1.76(−5)	
	90	0.002 39	7.59(−5)	− 0.0196	0.003 62	1.60(−5)	
	120	0.010 4	−9.34(−4)	− 0.0195	0.002 29	1.96(−5)	
	150	0.016 7	−0.001 42	− 0.0192	0.001 72	2.60(−5)	
	180	0.019 1	−0.001 56	− 0.0191	0.001 56	2.91(−5)	
1330	0	−81.0	0.062 7	−81.0	0.062 7	522.	0.484
	10	− 2.02	0.047 2	− 2.07	0.053 6	0.332	
	30	− 0.309	0.006 91	− 0.395	0.026 8	0.010 0	
	60	− 0.003 20	0.002 43	− 0.0768	0.015 4	2.44(−4)	
	90	0.023 0	0.002 06	− 0.0402	0.009 63	8.88(−5)	
	120	0.027 8	−1.07(−4)	− 0.0341	0.005 54	7.80(−5)	
	150	0.030 9	−0.001 87	− 0.0326	0.003 24	8.07(−5)	
	180	0.032 2	−0.002 51	− 0.0322	0.002 51	8.29(−5)	
1170	0	−81.0	0.072 6	−81.0	0.072 6	521.	0.624
	10	− 2.55	0.057 7	− 2.60	0.064 2	0.526	
	30	− 0.405	0.010 8	− 0.506	0.034 8	0.016 7	
	60	− 0.018 0	0.001 07	− 0.113	0.018 8	5.32(−4)	
	90	0.032 2	0.001 71	− 0.0552	0.011 4	1.67(−4)	
	120	0.037 6	4.04(−5)	− 0.0442	0.006 30	1.35(−4)	
	150	0.039 8	−0.001 71	− 0.0414	0.003 35	1.31(−4)	
	180	0.040 7	−0.002 39	− 0.0407	0.002 39	1.32(−4)	
1120	0	−81.0	0.064 6	−81.0	0.064 6	521.	0.684
	10	− 2.75	0.052 1	− 2.80	0.057 7	0.610	
	30	− 0.438	0.010 5	− 0.546	0.032 2	0.019 5	
	60	− 0.022 7	2.77(−4)	− 0.129	0.017 2	6.93(−4)	
	90	0.035 7	0.001 04	− 0.0624	0.010 3	2.09(−4)	
	120	0.042 0	−1.17(−4)	− 0.0490	0.005 66	1.67(−4)	
	150	0.043 9	−0.001 51	− 0.0455	0.002 95	1.59(−4)	
	180	0.044 6	−0.002 07	− 0.0446	0.002 07	1.59(−4)	
889	0	−81.0	0.100	−81.0	0.100	522.	1.08
	10	− 3.67	0.084 9	− 3.74	0.092 5	1.09	
	30	− 0.591	0.023 0	− 0.739	0.058 2	0.035 7	
	60	− 0.052 2	−0.004 86	− 0.238	0.030 5	0.002 40	
	90	0.053 7	−0.003 60	− 0.113	0.018 4	6.39(−4)	
	120	0.069 3	−0.003 19	− 0.0825	0.010 5	4.66(−4)	
	150	0.071 3	−0.003 98	− 0.0738	0.005 92	4.21(−4)	
	180	0.071 7	−0.004 40	− 0.0717	0.004 40	4.10(−4)	

TABLE VII. (*Continued*)

ω (keV)	θ (deg)	Elastic Amplitudes (R + NT) in r_0 Re$A_{\parallel}$	Im$A_{\parallel}$	Re$A_{\perp}$	Im$A_{\perp}$	$\frac{d\sigma}{d\omega}$ (barn/sr)	$\sigma(\omega)$ (barns)
662	0	−81.1	0.141	−81.1	0.141	522.	1.94
	10	− 5.03	0.125	− 5.12	0.134	2.05	
	30	− 0.855	0.046 4	− 1.06	0.095 9	0.073 8	
	60	− 0.133	−0.014 1	− 0.454	0.052 1	0.008 99	
	90	0.080 7	−0.016 4	− 0.239	0.031 4	0.002 58	
	120	0.129	−0.012 0	− 0.168	0.019 1	0.001 80	
	150	0.140	−0.009 98	− 0.147	0.011 9	0.001 54	
	180	0.141	−0.009 54	− 0.141	0.009 54	0.001 59	
412	0	−81.1	0.266	−81.1	0.266	523.	4.97
	10	−10.1	0.248	−10.3	0.259	8.29	
	30	− 2.08	0.136	− 2.48	0.217	0.418	
	60	− 0.312	−0.018 9	− 0.882	0.142	0.035 6	
	90	0.128	−0.062 9	− 0.607	0.093 1	0.015 8	
	120	0.313	−0.058 1	− 0.469	0.064 6	0.012 9	
	150	0.377	−0.047 7	− 0.408	0.048 8	0.012 4	
	180	0.391	−0.043 6	− 0.391	0.043 6	0.012 3	
279	0	−81.2	0.482	−81.2	0.482	524.	10.6
	10	−14.7	0.459	−15.0	0.475	17.5	
	30	− 3.50	0.307	− 4.14	0.429	1.18	
	60	− 0.625	0.023 7	− 1.56	0.328	0.116	
	90	0.155	−0.127	− 0.979	0.245	0.042 0	
	120	0.510	−0.162	− 0.821	0.190	0.039 5	
	150	0.681	−0.156	− 0.750	0.160	0.042 7	
	180	0.729	−0.150	− 0.729	0.150	0.044 0	
145	0	−81.2	1.40	−81.2	1.40	524.	35.8
	10	−28.5	1.36	−28.9	1.39	65.6	
	30	− 8.38	1.09	− 9.77	1.35	6.70	
	60	− 1.91	0.416	− 4.10	1.22	0.880	
	90	0.133	−0.229	− 2.71	1.09	0.341	
	120	1.04	−0.647	− 1.92	0.989	0.245	
	150	1.42	−0.848	− 1.61	0.926	0.245	
	180	1.53	−0.904	− 1.53	0.904	0.250	
75.0	0	−79.9	0.878	−79.9	0.878	507.	94.2
	10	−44.8	0.857	−45.5	0.875	162.	
	30	−14.8	0.697	−17.2	0.853	20.5	
	60	− 4.04	0.285	− 8.42	0.791	3.49	
	90	0.159	−0.125	− 4.45	0.722	0.809	
	120	1.67	−0.413	− 3.17	0.664	0.535	
	150	2.39	−0.569	− 2.73	0.629	0.551	
	180	2.61	−0.616	− 2.61	0.616	0.569	
59.5	0	−80.6	1.31	−80.6	1.31	516.	150.
	10	−51.5	1.28	−52.3	1.31	214.	
	30	−19.9	1.06	−23.1	1.29	37.1	
	60	− 5.69	0.475	−11.8	1.21	6.92	
	90	0.229	−0.154	− 7.54	1.13	2.31	
	120	2.77	−0.631	− 5.27	1.06	1.47	
	150	3.85	−0.907	− 4.41	1.01	1.43	
	180	4.18	−0.996	− 4.18	0.996	1.47	

TABLE VII. (*Continued*)

ω (keV)	θ (deg)	Elastic Amplitudes (R + NT) in r_0 Re$A_{\parallel}$	Im$A_{\parallel}$	Re$A_{\perp}$	Im$A_{\perp}$	$\frac{d\sigma}{d\omega}$ (barn/sr)	$\sigma(\omega)$ (barns)
22.1	0	−81.0	6.94	−81.0	6.94	525.	695.
	10	−71.0	6.82	−72.1	6.93	410.	
	30	−43.3	5.90	−50.1	6.90	177.	
	60	−16.0	3.18	−32.3	6.79	53.8	
	90	0.192	−0.276	−23.0	6.64	22.7	
	120	9.31	−3.45	−18.3	6.51	18.9	
	150	14.2	−5.62	−16.3	6.41	21.5	
	180	15.8	−6.38	−15.8	6.38	23.0	

to decrease slightly as photon energy increases. For photon energies near or below the photoeffect edges, we understand the qualitative behavior of the real parts of the single-particle Rayleigh amplitudes to be like that displayed by Gavrila's nonrelativistic K-shell amplitudes in that singularities in the single-particle amplitudes occur at all energies corresponding to differences in bound-electron energy levels. These resonances are artificial when both bound levels are filled but are real and usually narrow on our keV energy scale when one of the bound levels is unoccupied.

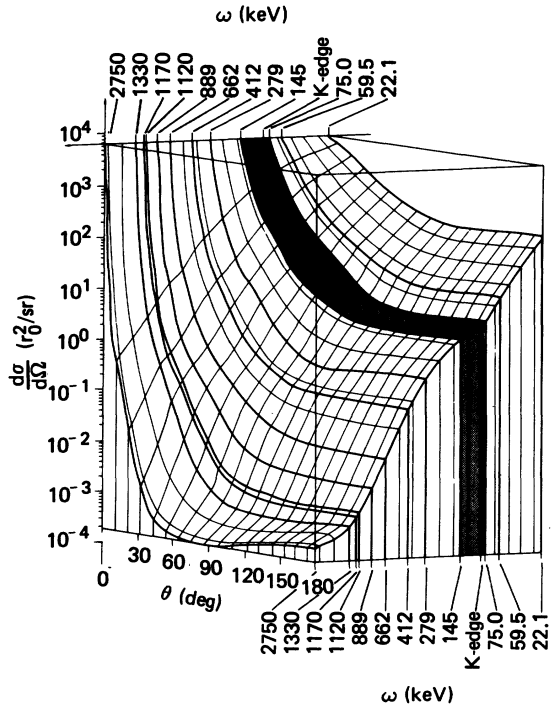

FIG. 17. A pseudo-three-dimensional plot of the differential elastic-photon-scattering cross sections of Table VII and Fig. 16. Data at photon energies intermediate to those listed in Table VII are found by logarithm-logarithm interpolation. The shaded area represents a region where there exist known singularities in the Rayleigh amplitudes.

The qualitative energy and Z dependence of the imaginary parts of the Rayleigh amplitudes are understood via the photoeffect cross section. As was stated earlier, for $\omega < 2\,mc^2 - \epsilon_K$ imaginary parts of the forward-Rayleigh-scattering amplitudes are analytically related to the photoeffect cross sections. The angular dependence of the imaginary amplitudes for a given electron is not qualitatively like that of the form-factor approximation for that electron. In form-factor approximation, the ratio of the contribution for two shells is equal to the ratios of numbers of electrons in the shells for small q and equal to the ratios of squared s-wave bound-state normalizations for large q [see equation (2.8)]. The ratios of the contributions to the imaginary amplitudes for two shells is found to be approximately constant independent of angle at least for the energies where it may be related to photoeffect. (See the review of the atomic photoeffect above 10 keV by Pratt, Ron, and Tseng.[53])

An important deviation from the form-factor approximation is found for the scattering of polarized photons. In the form-factor approximation, a zero is predicted at 90° for scattering of photons of linear polarization parallel to the plane of scattering (i.e., there exists a zero in $A_{\parallel}$). Our amplitudes strongly violate this prediction at all but the lowest energies. Instead of $A_{\parallel}$ going through zero at 90° as in the form-factor approximation, we find that Re($A_{\parallel}$) has a sign change usually well before 90° (as early as 67°) and that Im($A_{\parallel}$) has a sign change well before 90° (as early as 45°) for energies less than the pair-creation threshold at $2mc^2 - \epsilon_K$ and well after 90° (as late as 120°) for higher energies.

The nuclear Thomson amplitudes equation (4.2) provide a guide with which we can judge when the Rayleigh amplitudes become small enough to become unimportant. Figure 17 shows a flattening of our sample differential cross sections for large θ at the higher energies of 1.33 and 2.54 MeV. What we are witnessing is the Rayleigh amplitudes becoming small with respect to the nuclear Thom-

TABLE VIII. Shown is the division of the 82 electrons of neutral lead used for the tabulation of Table VII. In our prescription, the Rayleigh amplitudes for the inner electrons are found via a numerical evaluation of the second-order S matrix. The contribution to the real Rayleigh amplitudes for the outer electrons are estimated by the modified form-factor approximation for $q < 50$ Å^{-1} and by scaling S-matrix amplitudes for the K shell by form-factor ratios for $q > 50$ Å^{-1}. The contribution to the imaginary Rayleigh amplitudes for the outer electrons use the ratio of photoeffect cross sections to scale the imaginary S-matrix amplitudes for the inner electrons.

	Inner Electrons		Outer Electrons		
ω (keV)	Shells included	Number of electrons	Shells included	Number of electrons	$\sigma_{PE}^{outer}/\sigma_{PE}^{inner}$
2750	K	2	$L+M+N+O+P$	80	0.206
1330	$K+L$	10	$M+N+O+P$	72	0.0426
1170	K	2	$L+M+N+O+P$	80	0.213
1120	K	2	$L+M+N+O+P$	80	0.214
889	$K+L$	10	$M+N+O+P$	72	0.0434
662	$K+L$	10	$M+N+O+P$	72	0.0441
412	$K+L$	10	$M+N+O+P$	72	0.0452
279	$K+L+M$	28	$N+O+P$	54	0.0106
145	$K+L+M$	28	$N+O+P$	54	0.0111
75.0	$K+L+M$	28	$N+O+P$	54	0.0584
59.5	$K+L+M+N$	60	$O+P$	22	0.00966
22.1	$K+L+M$	28	$N+O+P$	54	0.0581

son amplitudes which are included in this tabulation. This occurs for lead at a momentum transfer of $q_{max} \simeq 80-150$ Å^{-1}. Thus, it is not necessary for us to dwell on the accuracy of the Rayleigh amplitudes for larger values of q. From our comparisons with the high-energy-limit predictions for the K shell, we expect the K-shell amplitudes tabulated by Florescu and Gavrila[32] to predict accurately the K shell for all momentum transfers of experimental interest for lead by several MeV. Thus for energies greater than several MeV, we may predict accurately the total-atom Rayleigh amplitudes to $O(2\%)$ by using K-shell amplitudes based upon the high-energy predictions of Florescu and Gavrila and estimating the contribution of higher shells as described earlier. In this sense we have made an explicit connection of our results with a high-energy-limit prescription.

TABLE IX. A comparison of forward scattering amplitudes predicted using our total atom prescription with those predicted using the anomalous scattering factors published by Cromer and Liberman (Ref. 30). As noted in equation (4.3) for forward scattering, $A_{\parallel}^{R} = A_{\perp}^{R}$.

		$f_0 + \Delta f' = -\mathrm{Re}A^R$			$\Delta f'' = -\mathrm{Im}A^R$		
atom	ω (keV)	This work	Cromer and Liberman	Relative difference (%)	This work	Cromer and Liberman	Relative difference (%)
^{13}Al	5.41	13.320	13.318	0.0	−0.514	0.522	1.6
	8.04	13.209	13.204	0.0	−0.243	0.246	1.2
	22.1	13.039	13.032	0.1	−0.031	0.031	0.0
^{30}Zn	5.41	29.161	29.316	0.5	−1.370	1.373	0.2
	8.04	28.369	28.388	0.1	−0.678	0.678	0.0
	22.1	30.323	30.260	0.2	−0.932	0.938	0.6
^{47}Ag	8.04	47.075	46.940	0.3	−4.242	4.282	0.9
^{62}Sm	8.04	58.307	56.304	3.4	−12.16	12.320	1.3
^{73}Ta	22.1	72.625	72.063	0.8	−4.403	4.399	0.1
^{82}Pb	22.1	80.966	80.090	1.1	−6.937	6.930	0.1

TABLE X. The total cross section $\sigma(\omega)$ for lead ($Z=82$) computed using our prescription for total-atom Rayleigh amplitudes (labeled "This work") is compared with form-factor-approximation predictions. The form-factor cross-section labeled "DHFS" are evaluated using the wave functions and potentials used in our prescription. (They agree to three significant figures with those interpolated from the relativistic 1979 tabulation of Hubbel *et al.*, Ref. 27.) The form-factor cross sections labeled "HUB75" are found by interpolation from the nonrelativistic 1975 tabulation of Hubbell *et al.* (Ref. 27). We note that the nonrelativistic form-factor predictions generally more closely approximate our results than the corresponding relativistic form-factor predictions. These cross sections do not include the amplitudes due to nuclear Thomson, nuclear-resonance, and Delbrück scattering.

	$\sigma(\omega)$ (barns/atom)				
ω (keV)	This work	Form factor DHFS	Relative difference (%)	Form factor HUB75	Relative difference (%)
2750	0.128	0.139	8.6	0.123	−3.9
1330	0.480	0.585	22.	0.520	8.3
1170	0.619	0.753	22.	0.669	8.1
1120	0.678	0.823	21.	0.729	7.5
889.	1.07	1.29	21.	1.15	7.5
662.	1.93	2.30	19.	2.04	5.7
412.	4.94	5.69	21.	5.07	2.6
279.	10.6	11.7	10.	10.6	0.0
145.	35.7	38.2	7.0	34.9	−2.2
75.0	94.0	118.	26.	110.	17.
59.5	150.	171.	14.	161.	7.3
22.1	695.	708.	1.9	687.	−1.2

Interpolating these results to other Z and ω for energies above the photoeffect K edge, we expect the Rayleigh amplitudes predicted via our prescription to be a smooth function of Z, ω. However, one cannot interpolate these predictions across photoeffect edges due to the existence of real resonances in the Rayleigh amplitudes from resonant bound-bound transitions between the occupied bound subshells to unoccupied bound states. We have prepared the pseudo-three-dimensional plot in Fig. 17 by linearly interpolating the logarithm of the differential cross section as a function of the logarithm of the energy (i.e., logarithm-logarithm interpolation). The shaded region of this figure indicates a region for which we have interpolated our cross sections across the photoeffect K edge. The interpolation in this region cannot be correct, and we caution others about this feature. Between the photoeffect K and L edges, such an interpolation should be valid well away from the edges.

V. COMPARISON WITH EXPERIMENT

In this section we compare results of our prescription for the prediction of accurate total-atom Rayleigh-scattering amplitudes with some recent experiments in the range of photon energies 1 keV–10 MeV. In reviewing comparisons between experiments and previous theory, we find that large (factor of two) discrepancies are restricted to photon energies below 100 keV and above 1 MeV. The energy region of 100 keV–1 MeV has recently been considered by Johnson and Cheng,[14] who compared differential elastic-scattering cross sections predicted by combining inner-shell Rayleigh amplitudes resulting from their numerical evaluation of the second-order S matrix and theoretical nuclear Thomson amplitudes with experiments of Schumacher *et al.*[54] They found 5% average differences between theory and experiment for heavy atoms (lead, $Z=82$) which grew to 20% average differences for light atoms (zinc, $Z=30$). They attributed the differences to the contributions made by outer electrons which were neglected in their theoretical cross sections.

Our new calculations remove the remaining large discrepancies between theory and experiment. We divided the energy range of interest into three regions. For photon energies greater than about 2 MeV, the Rayleigh amplitudes are dominant only for very small scattering angles. For these high energies, we expect our numerical K-shell Rayleigh amplitudes to closely approach the high-energy-limit predictions of Florescu and Gavrila[32] even for heavy atoms at all momentum transfers for which the Rayleigh amplitudes are important. For the intermediate energy range of 100 keV–2 MeV, the Rayleigh amplitudes dominate the elastic-scattering amplitude for most scattering angles, and the photon energy is typically large compared with electron binding energy. In the low-energy

region below 100 keV, the Rayleigh amplitude is essentially the sole component of the elastic-scattering amplitude. Here the photon energy is comparable or less than electron binding for heavy atoms.

To compare theory with experiment in the entire range 100 eV–10 MeV, we must include the amplitudes due to the other coherent-scattering processes where they are significant. Table XI indicates our expectations for a heavy atom such as lead, the relative importance of the four coherent processes that contribute to elastic photon scattering in this energy range. By making suitable choices for the variables Z, ω, and θ, one can perform experiments for which only one of the processes is predicted to contribute significantly. Berant *et al.*[55] have justified the use of the classical formula equation (4.2) for prediction of the nuclear Thomson amplitudes. The usual procedure of calculating the nuclear-resonance amplitudes by use of the giant-dipole-resonance (GDR) parameters extracted from photonuclear-absorption data have been justified by other measurements.[56,57] We may write the nuclear-resonance amplitudes in the units used for our Rayleigh amplitudes and nuclear Thomson amplitudes (the classical electron radius r_0) as

$$A_{\perp}^{\mathrm{NR}}=\sum_j \frac{\omega^2\sigma_j\gamma_j}{4\pi\alpha}\left(\frac{(\omega_j^2-\omega^2)+i\gamma\omega}{(\omega_j^2-\omega^2)^2+\gamma_j^2\omega^2}\right), \qquad A_{\parallel}^{\mathrm{NR}}=A_{\perp}^{\mathrm{NR}}\cos\theta, \tag{5.1}$$

where the sum is over the number of Lorentzian curves which are fit to the photonuclear absorption data (usually $j=1$ or 2). Here we use the notation: σ_j is the peak nuclear photoabsorption cross section of the jth resonance measured in units of squared electron Compton wavelengths $\lambda\!\!\!^{-2}\simeq 1.49\times10^6$ mb; ω_j the energy of the jth resonance measured in units of $mc^2\simeq 511$ keV; and γ_j the width of the jth resonance measured in units of $mc^2\simeq 511$ keV. The best available Delbrück amplitudes are those predicted by Papatzacos and Mork,[52] calculated in the lowest nonvanishing Born approximation for the point Coulomb potential, and so most appropriate for light elements at high energies if screening efforts may be neglected.

A. High-energy experiments (2.75-11.4 MeV)

Recent measurements of the elastic-scattering cross sections for photons of energies 6.84–11.39 MeV incident on lead and uranium scattered through 1.5° have been reported by Kahane *et al.*[6] Using K-shell high-energy-limit Rayleigh amplitudes due to Florescu and Gavrila,[32] the relativistic form-factor approximation to estimate the contribution of the electrons in the L and higher shells to the Rayleigh amplitudes, and Delbrück amplitudes provided by Papatzacos and Mork, Kahane *et al.* found good agreement between theory and experiment except for the 6.84-MeV measurement. The nuclear-resonance and nuclear Thomson amplitudes are very small here. The Rayleigh amplitudes dominate this lowest-energy experiment, and it is the L shell which dominates the Rayleigh contribution. For higher energies, where there is no discrepancy, the K shell is beginning to dominate the Rayleigh amplitude. For these energies and angles, the Delbrück amplitudes never strongly dominate the scattering. Papatzacos[52] has argued that the Coulomb corrections to his Delbrück amplitudes at higher energies will be smaller than at 2.75 MeV, where they appear to be responsible for a discrepancy. (See below.) Section III verified that high-energy-limit K-shell Rayleigh amplitudes

TABLE XI. The four coherent amplitudes that contribute to elastic scattering for 100 eV $<\omega<$ 10 MeV and their expected relative importance for various energy ranges for a heavy atom such as lead ($Z=82$).

Photon energy	Rayleigh A^{R}	Nuclear Thomson A^{NT}	Nuclear resonance A^{NR}	Delbrück A^{D}
10 MeV–3 MeV	dominates only at very small θ, becomes unimportant at large θ	important at intermediate and large θ [a]	important at intermediate and large θ	important at intermediate and large θ
3 MeV–1 MeV	dominates at smaller θ, important at intermediate θ	important at intermediate and large θ	important at intermediate and large θ	important at intermediate θ
1 MeV–100 keV	dominates at most θ	important at larger θ	unimportant	contributes
100 keV–100 eV	dominates at all θ	unimportant	unimportant	unimportant

[a]Intermediate angles have a range from 10° to 100°.

are accurate at these energies. In comparisons between our numerical Rayleigh amplitudes and the high-energy-limit amplitudes for the K shell, we found convergence to within 1% by $\omega = 3$ MeV for this momentum transfer of 7.2 Å^{-1}. Following our prescription for accurate total-atom Rayleigh amplitudes which we detailed in Sec. IV, we would use the modified form-factor approximation to estimate the contribution made by the L and higher shells to $\mathrm{Re}A^R$. The L-shell Rayleigh amplitudes predicted in this manner by the modified form factor are 15% smaller than those given by the form-factor approximation for uranium at 7.2 Å^{-1}. This confirms the explanation of the discrepancy offered by Kahane *et al.*; namely, that the form factor overestimates the contribution of the L and higher shells. Using our prescription for the total-atom Rayleigh amplitudes (i.e., the high-energy-limit K-shell amplitudes plus modified form factor estimates for the L and higher shells), and including the Delbrück amplitudes of Papatzacos and Mork, we predict differential scattering cross sections of 481 and 591 mb/sr for scattering 6.84 MeV photons through 1.5° by lead and uranium, respectively. This compares well with the experimental values of 471 ± 25 and 633 ± 61 mb/sr, respectively.

At 2.75 MeV, Schumacher *et al.*[5] have measured the differential elastic-scattering cross section for lead ($Z = 82$) and uranium ($Z = 92$) and found substantial disagreement with theory by factors of nearly two at the intermediate angles 30°–150°. The theoretical cross sections they used in the comparison include: the nuclear Thomson amplitudes equation (4.2), nuclear resonance amplitudes equation (5.1) using the GDR parameters of Veyssiere *et al.*,[58] Delbrück amplitudes supplied by Papatzacos and Mork, and Rayleigh amplitudes. For lead they simply used the mercury ($Z = 80$) K-shell amplitudes calculated by Cornille and Chapdelaine[35] at 2.62 MeV without correcting for the energy and atomic number. They argue that these corrections are of the same order as the contributions made by electrons not in the K shell. For the uranium comparison they used K-shell amplitudes supplied by us and used ratios of form factors to scale the K-shell amplitudes to estimate the contribution of the L shell. At this energy for these heavy atoms, all four coherent amplitudes are of roughly similar orders of magnitude. Rayleigh amplitudes calculated via our prescription detailed in Sec. IV do not substantially alter the result of their comparison, since it is only at the forward angles $\gtrsim 15°$ that the Rayleigh amplitudes dominate the elastic cross section. Schumacher *et al.* convincingly argue from angle and atomic-number dependence that the large differences between theory and experiment are caused by Coulomb corrections to the Delbrück amplitudes of Papatzacos and Mork, which were calculated in lowest-order Born approximation. At smaller angles (where the Rayleigh amplitudes dominate the cross section) and at larger angles (where the nuclear Thomson amplitudes dominate the cross section) the agreement between theory and experiment grew.

B. Intermediate-energy experiments (145 keV-1.33 MeV)

For the photon energy of 1.33 MeV, Dixon and Storey[2] and other experimenters[3,4,59] in their comparisons of theory and experiment for heavy atoms report discrepancies approaching a factor of 2 at large angles. At this energy, the Rayleigh K-shell amplitude is dominant at most angles. The theoretical Rayleigh amplitudes in these comparisons are all based on the numerical calculation of Brown and Mayers[11] for the K shell of mercury ($Z = 80$) at 1.31 MeV. Figure 18 compares these four experiments with theoretical differential cross sections which include our Rayleigh amplitudes, Delbrück amplitudes of Papatzacos and Mork,[52] nuclear Thomson amplitudes equation (4.2), and nuclear-resonance amplitudes equation (5.1) using the GDR parameters of Veyssiere *et al.*,[58] Our Rayleigh amplitudes are prepared according to the prescription of Sec. IV. Our calculation removes the large discrepancy; we now have good agreement for all angles. The introduction of artificial 3% errors in the dipole terms of our K-shell calculation induced errors in the differential scattering amplitudes similar to the discrepancy with

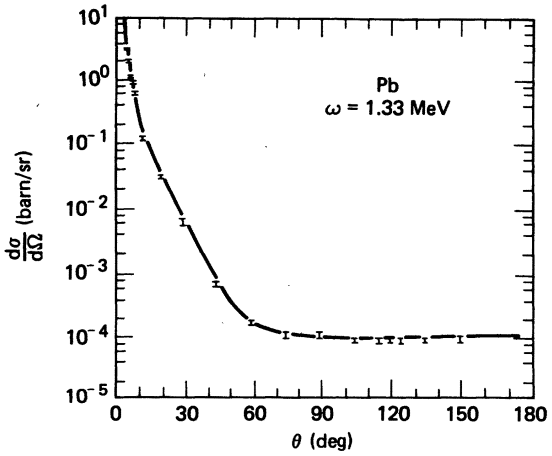

FIG. 18. Comparison of theory and several experiments (Refs. 2–4, 59) for lead at 1.33 MeV. Our calculation removes the large factor-of-two discrepancy with previous theory which occurred at large scattering angles, $\theta > 90°$.

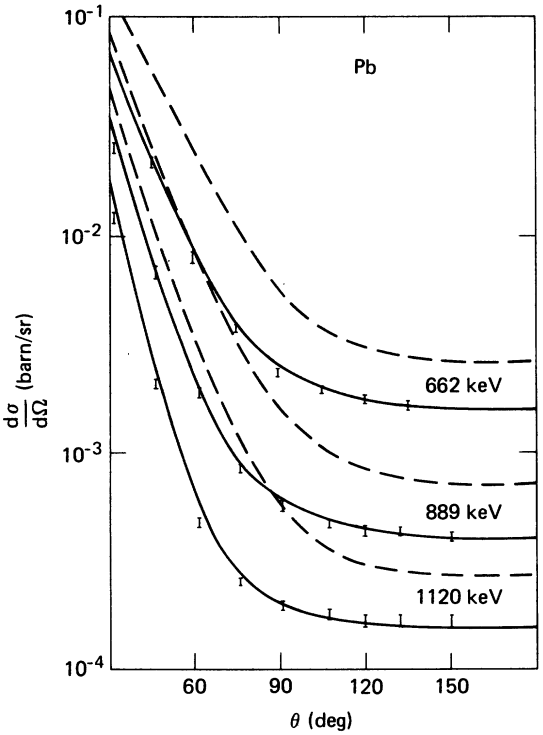

FIG. 19. Comparison of this theory (solid curves) and experiment (Ref. 54) for ^{82}Pb at the intermediate photon energies of 1120, 889, and 662 keV. We also display predictions based on the DHFS form factor (broken curves) for comparison.

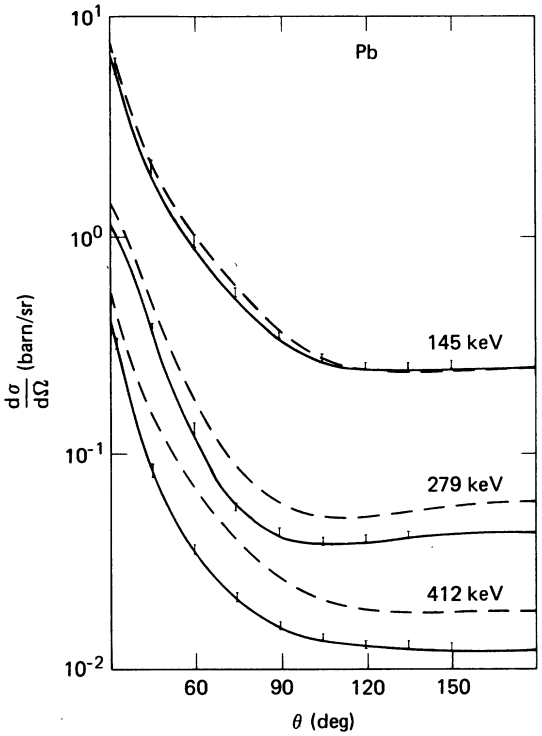

FIG. 20. Comparison of this theory (solid curves) with experiment (Ref. 54) for ^{82}Pb at the intermediate photon energies of 412, 279, and 145 keV. We also display predictions based on the DHFS form factor (broken curves) for comparison.

Brown and Mayers. This suggests that an accuracy of about 3% is maintained in the evaluation of their radial matrix elements. Because of destructive interference at large angles, cancellation among the multipole amplitudes can result in a factor-of-two error from this seemingly small 3% error. Such large errors do not affect Brown's other calculations since these interference effects are less pronounced at lower energy. We removed the discrepancy between theory and experiment without modifying the fundamental phase relationships among the various coherent amplitudes contrary to a suggestion made by Dixon and Storey.

Figures 19 and 20 compare theory with measurements of the differential cross sections made by Schumacher *et al.*[54] for 1120-, 889-, 662-, 412-, 279-, and 145-keV photons scattered by lead ($Z=82$). For these comparisons the theoretical cross sections are taken from those tabulated in Sec. IV and include the Rayleigh and nuclear Thomson amplitudes only. We note that the Delbrück amplitudes not available to us have affected the differential scattering cross sections at 1.33 MeV by 20%. As is noted in Sec. IV, the theoretical Rayleigh amplitudes tabulated here for 1120 keV approximate the contribution of the L shell, which introduces errors that increase the resulting theoretical cross sections by an amount we estimate to be $O(2\%)$. We find disagreement with experiment outside twice the reported experimental error for 30–60° at 1120 keV, 32° at 889 keV, and 45° at 662 keV. These discrepancies are not explained by the expected uncertainties in our theoretical cross sections. We might expect, as has been suggested by Mückenheim and Schumacher (private communication), that the Delbrück amplitudes must still be considered in this energy range. We have partially verified this by inserting the low energy limit of the Delbrück amplitudes[52] (valid in the forward direction) which appears to remove these discrepancies at forward angles.

C. Low-energy experiments (35-75 keV)

At photon energies below 100 keV, in the absence of better predictions, experimental measurements[8,9] have been compared with the form-factor approximation. We report theoretical predictions in good agreement with these experiments, and attribute the previous differences to the breakdown of the form-factor approximation for the K-shell contribution to the scattering. (See discus-

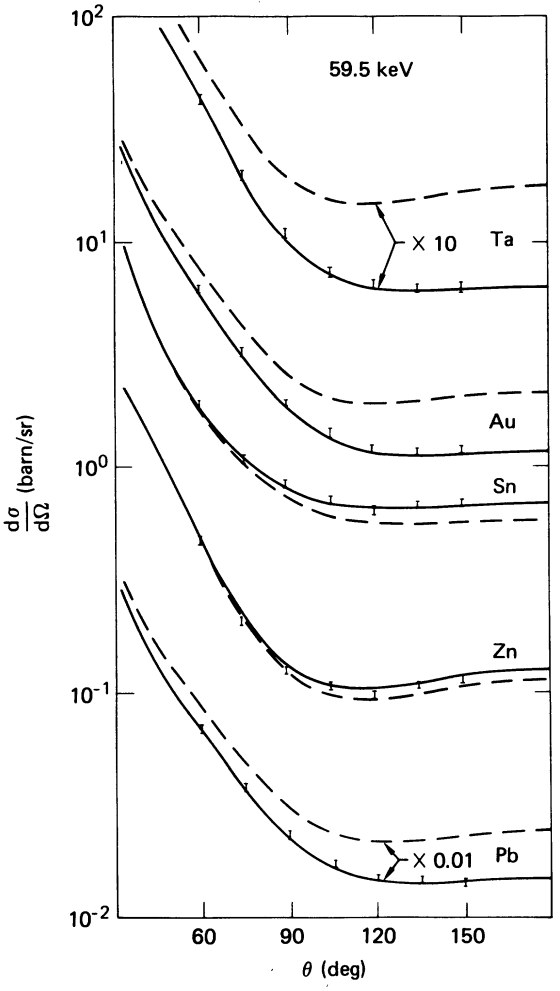

FIG. 21. Comparison of this theory (solid curves) with experiment (Ref. 8) for 59.5 keV photons incident on several elements from ^{30}Zn through ^{82}Pb. We also display predictions based on the DHFS form factor (broken curves) for comparison.

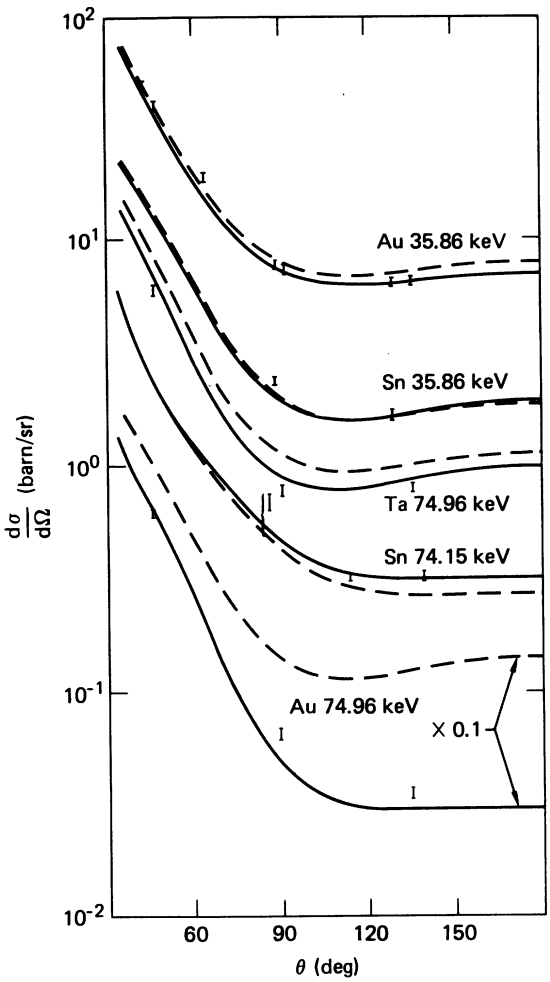

FIG. 22. Comparison of this theory (solid curves) with experiment (Ref. 9) for photon energies of 36 and 75 keV. We also show predictions based on the DHFS form factor (broken curves) for comparison.

sion in Secs. III and IV.) Comparisons of our numerical results with the experiment of Schumacher and Stoffregen[8] for a fixed photon energy of 59.5 keV and atomic numbers 30 through 82 in Fig. 21 shows good agreement at the 5% or better level, in marked contrast to the form-factor predictions. The largest discrepancy with the predictions of the form-factor approximation is found in the experiment for Ta ($Z=73$), which is the element whose K-shell binding energy of 67.4 keV is closest to 59.9 keV. At larger angles for this energy, the K shell dominates the total-atom form factor. Note that at smaller angles the agreement between experiment and form-factor predictions is improving since L and higher shells are becoming more important and these higher shells are more accurately predicted by the form factor at this energy. Our predictions for these low-energy cases are based on Rayleigh amplitudes derived from a numerical calculation of the second-order S matrix for the K-, L-, and M-shells.

In comparison with a recent experiment by Tirsell *et al.*,[9] for 35- and 75-keV photons scattered by tin ($Z=50$), tantalum ($Z=73$), and gold ($Z=79$) we find generally satisfactory agreement, but note larger differences especially at 90°. Figure 22 displays this comparison along with predictions of the form-factor approximation. Although the agreement between our predictions and this experiment is less satisfactory than for the 59.5-keV experi-

ment, our predictions still represent a large improvement over those of the form-factor approximation. Our predictions are again based upon numerical evaluation of the second-order S matrix for K-, L-, and M-shell electrons. Note that the agreement is substantially better than that Tirsell *et al.* found with the anomalous-dispersion corrections of Cromer and Liberman.[30] We found earlier that the anomalous scattering factors at forward angles provided excellent predictions as compared with amplitudes from our prescription. Preliminary investigation[60] of the methods commonly used to transform the forward-angle predictions of the anomalous scattering factor to other angles have not shown good agreement with our predictions.

ACKNOWLEDGMENTS

We would like to thank Dr. Walter Johnson and Dr. Chien-ping Lin for sharing with us their analytic and numerical methods, and Dr. Mihai Gavrila and Dr. Martin Schumacher for many useful discussions and valuable suggestions. We also wish to thank the staff of the Computer Center, University of Pittsburgh, for its extended help. This work was performed under the asupices of the U. S. Department of Energy. It was supported in part by the Department of Energy under Contract No. W-7405-Eng-48 with Lawrence Livermore Laboratory, including subcontract No. 9 776403, and in part by National Science Foundation under Grant No. PHY74-03 531 A03.

---

*Present address: Sandia National Laboratories, Albuquerque, New Mexico 87185.

†On leave from Bose Institute, Calcutta 700 009, India.

[1]W. D. Brown (Boeing Company, Seattle, Wash., Report No. D2-125136-1, 1966).

[2]W. R. Dixon and R. S. Storey, Can. J. Phys. 46, 1153 (1968).

[3]G. Hardie, W Merrow, and D. Schwandt, Phys. Rev. C 1, 714 (1970); G. Hardie, J. DeVries, and C. Chiang, *ibid.* C 3, 1287 (1971).

[4]G. Basavaraju and P. P. Kane, Nucl. Phys. A149, 49 (1970).

[5]M. Schumacher, F. Smend, and I. Borchert, Phys. Rev. C 13, 2318 (1976); M. Schumacher and P. Rullhusen, Phys. Lett. 71B, 276 (1977).

[6]S. Kahane, O. Shahal, and R. Moreh, Phys. Lett. 66B, 229 (1977).

[7]S. Kahane, R. Moreh, and O. Shahal, Phys. Rev. C 18, 1217 (1978).

[8]M. Schumacher and A. Stoffregen, Z. Phys. A 283, 15 (1977).

[9]K. G. Tirsell, V. W. Slivinsky, and P. J. Ebert, Phys. Rev. A 12, 2426 (1975).

[10]J. W. Strutt, Philos. Mag. 41, (Ser. 4), 107 (1871); 41, (Ser. 4), 274 (1871); 41 (Ser. 4), 447 (1871).

[11]G. E. Brown, R. E. Peierls, and J. B. Woodward, Proc. R. Soc. London A227, 51 (1955); S. Brenner, G. E. Brown, and J. B. Woodward, *ibid.* A227, 59 (1955); G. E. Brown and D. F. Mayers, *ibid.* A234, 387 (1955); A242, 89 (1957).

[12]A preliminary report on some of these results was given in L. Kissel and R. H. Pratt, Phys. Rev. Lett. 40, 387 (1978). This work is based on results reported in L. Kissel, thesis, University of Pittsburgh, 1977 (unpublished); L. Kissel and R. H. Pratt, Lawrence Livermore Laboratory, Internal Report No. XRM-78-107 (unpublished); L. Kissel, *ibid.* XRM-79-7 (unpublished); *ibid.* XRM-80-4 (unpublished); *ibid.* XRM-80-82 (unpublished); *ibid.* XRM-80-83 (unpublished); S. C. Roy and R. H. Pratt, University of Pittsburgh, Internal Report No. Pitt-230 (unpublished).

[13]W. R. Johnson and F. D. Feiock, Phys. Rev. 168, 22 (1968); F. D. Feiock and W. R. Johnson, *ibid.* 187, 39 (1969); Chien-ping Lin, Kwok-tsang Cheng, and W. R. Johnson, Phys. Rev. A 11, 1946 (1975).

[14]W. R. Johnson and Kwok-tseng Chang, Phys. Rev. A 13, 692 (1976).

[15]M. Gavrila (private communication), FOM Institute for Atomic and Molecular Physics, Kruislaan 407, Amsterdam-W, The Netherlands.

[16]D. Liberman, J. T. Waber, and D. T. Cromer, Phys. Rev. 137, A27 (1965).

[17]J. H. Hubbell, *Photon Cross Sections, Attenuation Coefficients, and Energy Absorption Coefficients from 10 keV to 100 GeV*, Natl. Bur. Std. (U.S.), Report No. NSRDS-NBS 29 (U.S. GPO, Washington D. C., 1969).

[18]R. W. James, *The Optical Principles of the Diffraction of x-Rays* (Bell, London, 1962), p. 94.

[19]See, for example, A. Sommerfeld, *Atombau und Spektrallinien* (Vieweg, Braunschweig, 1939), Vol. 2, Chap. 8, Secs. 5 and 6.

[20]W. Franz, Z. Phys. 95, 652 (1935); 98, 314 (1936).

[21]J. S. Levinger, Phys. Rev. 87, 656 (1952).

[22]K. Gottfried, *Quantum Mechanics* (Benjamin, New York, 1966), Vol. I, p. 153.

[23]J. D. Bjorken and S. D. Drell, *Relativistic Quantum Mechanics* (McGraw-Hill, New York, 1964), p. 131.

[24]We use the natural units $\hbar=m=c=1$ ($\hbar \simeq 6.58\times10^{-22}$ MeV sec is Planck's constant, $m \simeq 0.511$ MeV/c^2 is the electron's rest mass, and $c \simeq 3.00\times10^{10}$ cm/sec is the speed of light). We measure energy in units of the electron's rest mass energy ($mc^2 \simeq 0.511$ MeV), length in units of the electron's Compton wavelength ($\lambda=\hbar/mc \simeq 3.86\times10^{-11}$ cm), and time in units of the interval required for light to travel one electron Compton wavelength ($\hbar/mc^2 \simeq 1.29\times10^{-21}$ sec). The fine-structure constant is $\alpha=e^2/\hbar c \simeq \frac{1}{137}$, and the classical electron radius is $r_0=e^2/mc^2 \simeq 2.82\times10^{-13}$ cm. The momentum transfer measured in Å^{-1} is obtained from q in mc by multiplying by the factor 20.61.

[25]Strictly speaking, the form-factor approximation includes some zeroth-order binding correction in that the electron charge density used is localized. This localization could be considered as some zeroth-or-

der binding effect. However, the form-factor approach neglects any further effects of binding on the scattering process.

[26]R. H. Pratt and H. K. Tseng, Phys. Rev. A 5, 1063 (1972).

[27]J. H. Hubbell, W. J. Veigele, E. A. Briggs, R. T. Brown, D. T. Cromer, and R. J. Howerton, J. Phys. Chem. Ref. Data 4, 471 (1975). Relativistic atomic form factors are available in J. H. Hubbell and I. Øverbø, J. Phys. Chem. Ref. Data 8, 69 (1979) based in part on the extended-range relativistic form factors by I. Øverbø, Nuovo Cimento 40B, 330 (1977); Phys. Scr. 17, 547 (1978).

[28]Brown and Mayers reported that use of $g(q)$ improved the amplitude for scattering of circularly polarized photons with no change of polarization A_{NSF} (no-spin-flip amplitude), but not the spin-flip amplitude A_{SF}. The scattering amplitudes for circularily polarized photons are related to the amplitudes for linear polarizations by $A_{SF}=\frac{1}{2}(A_{\parallel}-A_{\perp})$, $A_{NSF}=\frac{1}{2}(A_{\parallel}+A_{\perp})$.

[29]G. E. Brown and J. B. Woodward, Proc. Phys. Soc., London 65A, 977 (1952).

[30]D. T. Cromer and D. Liberman, J. Chem. Phys. 53, 1891 (1970); Los Alamos Scientific Laboratory Report No. LA-4403, 1970; D. T. Cromer, Acta Crystallogr. 18, 17 (1965).

[31]M. L. Goldberger and F. E. Low, Phys. Rev. 176, 1778 (1968).

[32]V. Florescu and M. Gavrila, Phys. Rev. A 14, 211 (1976).

[33]M. Gavrila, Phys. Rev. 163, 147 (1967).

[34]A. Costescu, Rev. Roum. Phys. 21, 3 (1976).

[35]H. Cornille and M. Chapdelaine, Nuovo Cimento 14, 1386 (1959).

[36]The symbols n, κ, m_j denote the bound-state quantum numbers [n = prinicipal quantum number, $\kappa = \mp(j+\frac{1}{2})$ as $j = l \pm \frac{1}{2}$ (or $j = l' \mp \frac{1}{2}$) is a quantum number which combines the total angular-momentum quantum number j and parity, and m_j is the projection of j in the z direction]. $E_{n\kappa}$ is the total energy of the state $|n\kappa m_j\rangle$ which includes the electron's rest mass and $\epsilon_{n\kappa} = E_{n\kappa} - 1$ is the binding energy. Again as detailed in Ref. 24, we work in the system of units with $\hbar = m = c = 1$.

[37]For a more detailed description of the form of the X amplitudes see Ref. 13.

[38]W. Kohn and L. S. Sham, Phys. Rev. 140, A1133 (1965).

[39]E. U. Condon and G. H. Shortley, *The Theory of Atomic Spectra* (Cambridge University Press, New York, 1970).

[40]M. Abramowitz and I. A. Stegun, *Handbook of Mathematical Functions* (Dover, New York, 1968).

[41]As suggested by G. E. Brown in a paper by J. S. Levinger and M. L. Rustgi, Phys. Rev. 103, 439 (1956), this pair-creation cross section enters Eq. (3.5) with a minus sign, since we are discussing the contribution made by a particular bound electron to elastic scattering. That is, we define the contribution of this particular electron as the difference in contributions due to the full atom (nucleus and all bound electrons) and the full atom with this electron missing (which we call the reduced atom). The imaginary part of the forward-scattering Rayleigh amplitude for a particular electron will then be proportional to the difference of the photoeffect cross sections plus the difference of the pair-production cross sections. The full-atom photoeffect cross section is larger than the reduced-atom photoeffect cross section due to the presence of this extra electron (hence the plus sign). The reduced-atom bound-electron pair-production cross section is larger than that for the full atom. This is due to the exclusion principle which will forbid the creation of an electron in an occupied state (hence the minus sign). See also T. Erber, Ann. Phys. (N.Y.) 6, 319 (1959).

[42]W. R. Johnson, D. J. Buss, and C. O. Carroll, Phys. Rev. 135, A1232 (1964); W. R. Johnson, *ibid.* 159, 61 (1967).

[43]H. K. Tseng and R. H. Pratt, Phys. Rev. A 7, 1423 (1973).

[44]J. H. Scofield, Lawrence Livermore Laboratory, Report No. UCRL-51326, 1973 (unpublished).

[45]A. Ron and H. K. Tseng, available from the Dept. of Physics, University of Pittsburgh, Report No. 6985207-17, 1971.

[46]Since the Rayleigh-scattering amplitudes are in general complex, the comparison has been simplified by considering the sum of squared amplitudes. For high photon energies, sign changes in the amplitudes cause confusing direct comparisons. At lower energies near but above the photoeffect edge, the values of the imaginary parts are large.

[47]Professor G. E. Brown (Department of Physics, State University of New York at Stony Brook, Stony Brook, N. Y. 11794) verified the possibility of the errors in his numerically generated amplitudes (about 5 or 6 places) due to the limited precision of the computer he used.

[48]As we discussed in Sec. II, the form factor is a high-energy approximation since one uses the Born approximation in its derivation. On the other hand, the exact single-particle matrix element Eq. (3.1) includes in its intermediate states $|p\rangle$ all eigenstates of the electron. For high photon energies the important intermediate states of the exact single-particle matrix element correspond closely (but not exactly) to the Born intermediate states of the form-factor approximation. However, at photon energies near the electron binding energies, the near-lying intermediate states tend to dominate the exact single-particle scattering amplitudes, making a direct comparison with form-factor predictions difficult to interpret. Note that results for the total-atom (summed over electrons) exact scattering amplitudes will tend to reduce the magnitude of this difficulty since contributions to Eq. (3.1) corresponding to transitions between two occupied bound states will cancel identically. Comparison with total-atom form-factor predictions will be presented in Sec. IV. This difficulty indicates that we must exercise caution when mixing various formalisms.

[49]Florescu and Gavrila investigated the validity of their high-energy-limit amplitudes at finite energy by comparisons with the numerical amplitudes of Brown *et al.*, (Ref. 11) Cornille and Chapdelaine (Ref. 35), and Johnson and Lin (private communication). They observed that their high-energy-limit amplitude gives a uniform approximation to the finite-energy matrix

element for energies ω from nonrelativistic to extremely high relativistic energies for $\omega \gg \epsilon$, and $(q/Z\alpha mc)^2 \ll O(\omega/mc^2)$.

[50]J. McEnnan, L. Kissel, and R. H. Pratt, Phys. Rev. A 13, 532 (1976); 14, 521 (1976).

[51]H. Brysk and C. D. Zerby, Phys. Rev. 171, 292 (1968).

[52]P. Papatzacos unpublished thesis (1974); P. Papatzacos and K. Mork, Phys. Rev. D 12, 206 (1975).

[53]R. H. Pratt, A. Ron, and H. K. Tseng, Rev. Mod. Phys. 45, 273 (1973).

[54]M. Schumacher, F. Smend, and I. Borchert, Nucl. Phys. A206, 531 (1973). F. Smend, M. Schumacher, and I. Borchert, Nucl. Phys. A213, 309 (1973); M. Schumacher, Phys. Rev. 182, 7 (1969).

[55]Z. Berant, R. Moreh, and S. Kahane, Phys. Lett. 69B, 281 (1977).

[56]T. Bar-Noy and R. Moreh, Nucl. Phys. A275, 151 (1977); Nucl. Instrum. Methods 105, 557 (1972).

[57]H. Jackson, G. Thomas, and K. Wetzel, Phys. Rev. C 9, 1153 (1974).

[58]A. Veyssiere, H. Beil, R. Bergere, P. Carlos, and A. Lepretre, Nucl. Phys. A159, 561 (1970); A. Veyssiere, H. Beil, P. Carlos, A. Lepretre, and K. Kernbath, Nucl. Phys. A199, 45 (1973).

[59]P. Kane, G. Basavaraju, J. Mahajani, and A. Priyadarsini, Nucl. Instrum. Methods 155, 467 (1978).

[60]L. Kissel, Lawrence Livermore Laboratory, Internal Report No. XRM-80-84 (unpublished).